A Modified Effective Stress Principle for Unsaturated Swelling Clays Derived from Microstructure

Julia Mainka, Marcio A. Murad, Christian Moyne, Sidarta A. Lima

A Modified Effective Stress Principle for Unsaturated Swelling Clays Derived from Microstructure

Julia Mainka[a,b*] Marcio A. Murad[c] Christian Moyne[a,b]
Sidarta A. Lima[c]

March 24, 2014

a) Université de Lorraine, LEMTA, UMR 7563, F-54500 Vandoeuvre-lès-Nancy, France

b) CNRS, LEMTA, UMR 7563, F-54500 Vandoeuvre-lès-Nancy, France

c) Laboratório Nacional de Computação Científica LNCC/MCT, Av. Getúlio Vargas 333, 25651-070 Petrópolis, RJ, Brazil

Executive Summary

We present an extension of the effective stress principle to unsaturated expansive clays characterized by two porosity levels (micro- and nanopores) including generalizations of the Bishop parameter, equivalent pore pressure and swelling stress. Such new quantities aim at capturing the coupled phenomena arising from the additional nanopore level.

Abstract

A three-scale model is proposed to describe electro-chemo-mechanical couplings in unsaturated swelling clays characterized by two porosity levels and three separate length scales. The nanoscale portrait consists of charged clay particles separated by a nanoporous network saturated by a binary monovalent aqueous electrolyte solution. Local ion distribution and electric potential are governed by the Poisson-Boltzmann problem. At the microscale, the system is represented by swollen clay clusters separated from each other by a network of micropores filled by a

* Corresponding Author; email: julia.mainka@univ-lorraine.fr; Co-authors: Marcio Arab Murad (murad@lncc.br), Christian Moyne (christian.moyne@univ-lorraine.fr), Sidarta Araujo de Lima (sidarta@lncc.br)

mixture of bulk water and air. Under mechanical equilibrium characterized by the competition between disjoining forces of electrochemical nature and capillary attraction effects, a novel form of the effective stress principle is derived in the asymptotic limit of scale separation. Such form includes a new macroscopic equivalent pore pressure weighted by a two-scale effective Bishop coefficient which incorporates the effects of the adsorbed water at the secondary nanopore level in addition to the contributions of the water air interfaces at the micropore level. Within the thermodynamic context for constructing macroscopic constitutive laws seated on stress-strain variables, the three-scale model leads to a set of three work-conjugated state variables. In addition to the contact stress between particles and the new effective Bishop-type component the novel form includes salinity as an additional stress-conjugated variable and a three-scale version of the electrochemical swelling stress. The potential of the multiscale approach in capturing the complex features of unsaturated expansive clays is illustrated by numerical reconstruction of the effective coefficients in a simplified isotropic microstructure.

Keywords: unsaturated swelling clay, homogenization electro-chemo-mechanical couplings, Bishop parameter, equivalent pore pressure disjoining (swelling) pressure, Poisson-Boltzmann, electric double layer

1 Introduction

Since the seminal works of Terzaghi and Biot who constructed the foundations of the effective stress principle for fully-saturated porous media several extensions with varying degree of sophistication have been proposed to unsaturated geomaterials (Alonso *et al.*, 1990, 1999; Gens and Alonso, 1992; Sheng *et al.*, 2004, 2008a,b; Borja and Koliji, 2009; Coussy *et al.*, 2010; Nuth and Laloui, 2008; Laloui and Nuth, 2009; Khalili *et al.*, 2004; Gallipoli *et al.*, 2003; Alonso *et al.*, 2010; Coussy and Brisard, 2009; Vlahinic *et al.*, 2011). The necessity of proper extensions to unsaturated states became a great challenge for the geotechnical community. Pioneer works put substantial efforts toward the proper identification of a single effective stress, commonly referred to as Bishop-type effective stress (Bishop, 1959; Sheng *et al.*, 2008b; Laloui and Nuth, 2009) where the Bishop parameter incorporates information regarding microstructure of the deformable medium and can be mainly envisioned as a scaling factor that captures the weight of the contribution of each fluid pressure to the effective stress. Subsequently it was recognized that the choice of the stress space to describe thermodynamically volume changes in unsaturated media turns out to be more complex. More precisely, an improved characterization of the mechanics was accomplished by the use of two independent sets of stress variables, namely the net stress and matric suction (Fredlund and Morgenstern, 1977) work-conjugated by the soil skeleton strain and the degree of saturation. The flexibility in the choice of the independent stress state variables along with the necessity of capturing smooth transition between unsaturated and saturated states have provided further insight in the subject

(Sheng *et al.*, 2008b; Houlsby, 1997; Nuth and Laloui, 2008; Gens, 1995). Such thermodynamic setting has been extended to elasto-plasticity by Alonso et al. (Alonso *et al.*, 1990, 1999) giving rise to the well-established Barcelona model of unsaturated soils. The Barcelona model was the forerunner of several other enhanced constitutive models widely adopted in modern theory of unsaturated soil mechanics, see for example (Vaunat *et al.*, 2000; Wheeler *et al.*, 2003; Sheng *et al.*, 2004, 2008a; Pereira *et al.*, 2005). More recently, the Bishop-based models and more general concept of effective stress were revised aiming at allowing a continuous transition between unsaturated and saturated state also reducing the number of constitutive model parameters (Houlsby, 1997; Loret and Khalili, 2002; Khalili *et al.*, 2004; Nuth and Laloui, 2008).

Despite the aforementioned advances to describe the stress partitioning mechanisms in unsaturated soils, to the best of authors knowledge, few works have attempted to extend the methodology to media composed of two levels of porosity. In particular, Borja (Borja and Koliji, 2009) developed a purely macroscopic theory based on first principles of thermodynamics by identifying energy-conjugate stress variables and obtained the effective stress principle with reference to the mean pressure weighted by the fluid phase saturations. When electrochemical effects are present in the secondary level of pores the adsorptive potentials associated with the water thin film behavior are lumped in the matric suction component. On the other hand, the issue of properly extending the thermodynamics to swelling clays highly sensitive to salinity (or more precisely to ion concentrations) and disjoining pressure remains an open issue. In spite of the well accepted incorporation of the electrochemical expansion stress in the effective stress principle (strongly dependent on ion concentration (Huyghe and Janssen, 1997, 1999; Schreyer-Bennethum, 2007)) the multiscale derivation of this quantity defined by the nanopore modeling seated on Poisson-Boltzmann based-theories was accomplished for fully-saturated clays (Murad and Moyne, 2002, 2008; Moyne and Murad, 2002). The extension to clayey soils with two levels of porosity, namely nano- and micropores with the latter partially saturated by water and air remains an open issue. The paper aims at filling this gap. Our main goal is to capture precisely the effects of the secondary level of nanopores fully-saturated by adsorbed water and construct a rigorous derivation of the modified effective stress principle for unsaturated expansive clays from nano- and microstructural behaviors of the colloidal system along with the precise determination of the constitutive responses of the effective Bishop parameter, equivalent pore pressure and swelling stress.

In order to avoid a possible misleading terminology and maintain consistency with the nomenclature commonly adopted, hereafter nanopores refer to the intra-aggregate pores whereas micropores to the inter-aggregate pores. Within the context of the three-scale setting, at the nanoscale the portrait of the soil fabric is an assembly of colloidal-size particles with lamellar structure with typical characteristic scale of the order of the Debye's length $\mathcal{O}(10^{-9}\,\mathrm{m})$ which measures the effective thickness of the electric double-layer (EDL) (Hunter, 1981). At this scale the electrolyte solution can still be regarded as a continuum fluid with ion distributions governed by the Poisson-Boltzmann equation. At

the microscale (the homogenized nanoscale), whose typical length is of $\mathcal{O}(10^{-6}\,\mathrm{m})$, the highly heterogeneous solid-fluid interactions are represented in an averaged fashion with the electrolyte solution and particles viewed as overlaying continua forming swollen clay clusters (or aggregates) with averaged properties established at every point of the mixture. The mechanisms governing the deformation of the solid matrix are ruled by the averaged stress partitioning rules which are dictated by the modified form of Terzaghi's effective stress principle incorporating the additional chemical expansion stress (Hueckel, 1992; Achari *et al.*, 1999). The microscopic two-scale chemo-mechanical model for the clay clusters is coupled with the bulk water which partially saturates the micropore system. Owing to the coarser structure of the micropores with larger size void spaces and characteristic length much greater than the Debye's length, the equations governing the bulk fluid are free of EDL effects. This particular feature distinguishes properties of a bulk fluid from an electrolyte solution and further implies in a pointwise form the electroneutrality condition with local equality between co- and counterion concentrations (Newman, 1973). To overcome the complexities that emerge from quantifying the role of interfacial phenomena on the overall stress we pursue the concept of the equivalent pore pressure based on the representation of the interfacial energy in terms of the area underneath the water retention curve (Coussy and Dangla, 2002; Coussy, 2010; Leverett, 1941; Grant and Gerhard, 2007). Such quantity plays the role of the pressure of an homogeneous equivalent fictitious fluid which produces the same mechanical response of the unsaturated case. It is commonly defined by weighted averaging using Bishop's effective stress coefficient (Loret and Khalili, 2000, 2002; Coussy and Dangla, 2002; Pereira *et al.*, 2005) (see Gray et al. (Gray and Schrefler, 2001; Gray *et al.*, 2009) for more general definitions). In contrast to the averaged pore pressure, which ignores the stresses induced by the interfacial energy upon the porous matrix, the equivalent pore pressure accounts for the excess in the surface energy which is essential to enforce local equilibrium (Coussy and Dangla, 2002; Dormieux *et al.*, 2006) and consequently leads to deviations of the Bishop parameter from saturation when selecting the weighted average parameter (Coussy and Dangla, 2002; Pereira *et al.*, 2005; Nikooee *et al.*, 2013). Recently, more refined rational thermodynamic approaches including balance and constitutive laws for the interfaces leading to non-Bishop type constitutive equation have been postulated. The outcome shows the contribution of interfacial area to the effective stress tensor and provides general representation for the equivalent pore pressure and Bishop coefficient (see e.g. (Nikooee *et al.*, 2013)).

By exploring the equivalent pore pressure concept the coupled micropore/cluster model is established at the microscale. Assuming local periodicity of the aggregates we apply the homogenization procedure to up-scale the coupled cluster/micropore model to the macroscale. This yields a novel form of the effective stress principle linked to local microscale problems posed in each clay cluster domain. By exploring the closure problems arising from the homogenization procedure we provide microscopic representations for the effective Bishop parameter, equivalent pore pressure and swelling pressure. Such representations furnish more refined information compared to their well-known two-scale formula

(Derjaguin *et al.*, 1987; Israelachvili, 1991; Loret and Khalili, 2002; Pereira *et al.*, 2005; Gray *et al.*, 2009; Nikooee *et al.*, 2013). In particular the feasibility of capturing precisely the influence of the additional level of nanoporosity upon the effective constitutive response of the macroscopic parameters.

The above multiscale procedure is solved numerically within the context of the self consistent homogenization methods considering a particular spherical isotropic microstructure. By solving the Poisson-Boltzmann equation numerically we construct constitutive laws for the three-scale swelling pressure, Bishop parameter and equivalent pore pressure which reproduce their classical two-scale behavior in the limit case where the influence of the additional pore level is neglected.

2 Two-scale model of the clay clusters

The framework of reiterated homogenization applied to double-porosity systems allows to rigorously derive the effective (macroscopic) behavior from the description of the phenomena at the nanoscopic clay particle scale (Auriault *et al.*, 2009; Sanchez-Palencia, 1980). Our aim here is to obtain explicit representations for the macroscopic swelling stress tensor $\boldsymbol{\Pi}_{eff}$ along with the Bishop parameter $\boldsymbol{\chi}^{eff}$ and the effective equivalent pore pressure tensor $\boldsymbol{P}_f^{eff} = (\boldsymbol{I} - \boldsymbol{\chi}^{eff})P_a + \boldsymbol{\chi}^{eff}P_w$ starting from the microstructural behavior.

For the sake of completeness we recall here the two-scale mechanics (nano/micro) for the clay clusters with nanopores fully saturated by an electrolyte solution composed of a water solvent and completely dissolved monovalent ions such as Na^+/Cl^- or K^+/Cl^- (Murad and Moyne, 2002). Ranges of very low moisture content in extreme dry clays are not considered here. Particles are assumed linear elastic undergoing quasi-static small deformations from an arbitrary reference configuration and contain a uniformly distributed negative surface charge density neutralized by the excess of positively charged dissociated ions to fulfill the electroneutrality condition. Swelling is solely due to the overlapping between adjacent double layers and effects of crystalline swelling are thoroughly neglected. The electrolyte solution is considered an incompressible structureless liquid with dissolved ions treated as point charges at thermodynamic equilibrium with the ions in the outer bulk water which partially saturates the micropores. According to the classical framework of homogenization (Auriault, 1990; Sanchez-Palencia, 1980), the nanoscopic governing equations are posed in a unit cell $Z = Z_l \cup Z_s$ composed by the subdomains occupied by the clay particles Z_s and the electrolyte solution Z_l, with an interface ∂Z_{ls} (Fig. 1). Salinity in the bulk fluid $C^+ = C^- = C$ and reference electric potential φ_b (assumed zero for convenience) are given quantities. The bulk water pressure P_w varies with the microscopic coordinate due to gravitational effects and therefore is independent of the nanoscopic location $\boldsymbol{z}$ (Murad and Moyne, 2002).

The averaging of the equilibrium equations of the fluid and solid subdomains yields the overall equilibrium of the clay clusters (Murad and Moyne, 2002) which when supple-

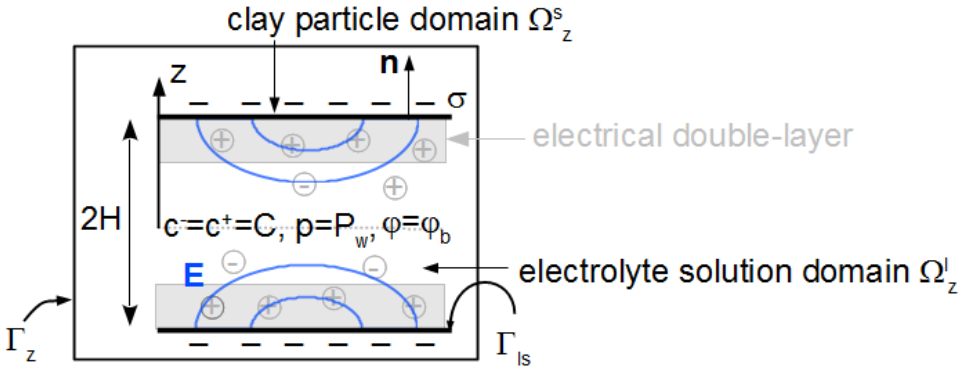

Figure 1: Nanoscopic portrait composed of the subdomains occupied by the clay particles Ω^s_z and electrolyte solution Ω^l_z.

mented by the body force results is given by

$$\boldsymbol{\nabla}_y \cdot \boldsymbol{\sigma}_t + \rho_t \boldsymbol{g} = 0 \qquad \text{in} \quad \Omega^s_y \,, \tag{1}$$

where $\boldsymbol{\sigma}_t$ is the total stress tensor of the clay clusters, $\boldsymbol{g}$ the gravity vector and ρ_t denotes the cluster density weighted by the intra-cluster porosity ϕ in terms of the water ρ_w and clay particle ρ_s densities in the form $\rho_t := \phi\rho_w + (1-\phi)\rho_s$. The modified effective stress principle for $\boldsymbol{\sigma}_t$ reads (Murad and Moyne, 2002)

$$\boldsymbol{\sigma}_t = -P_w \boldsymbol{I} + \boldsymbol{C}\boldsymbol{\mathcal{E}}_y(\boldsymbol{u}) - \boldsymbol{\Pi} \,, \tag{2}$$

where $\boldsymbol{I}$ is the unit tensor, $\boldsymbol{C}$ the effective elasticity tensor of the clay clusters, $\boldsymbol{\mathcal{E}}_y(\boldsymbol{u})$ the symmetric part of the gradient of the displacement $\boldsymbol{u}$ and $\boldsymbol{\Pi}$ the homogenized swelling stress tensor given by

$$\boldsymbol{\Pi} = \phi\langle \boldsymbol{\Pi}_d \rangle^l + (1-\phi)\langle \boldsymbol{\sigma}_\Pi \rangle^s \,, \tag{3}$$

with $\langle\cdot\rangle^{l(s)} = 1/\left|Z_{l(s)}\right| \int_{Z_{l(s)}} \cdot\, dZ$ the volume average operator over the fluid (solid) subdomain of the periodic cell Z. In what follows we describe each component of the swelling stress. The contribution of the electrolyte solution to the swelling tensor is the average over the fluid phase of the disjoining pressure (Moyne and Murad, 2002)

$$\boldsymbol{\Pi}_d := RT\left(c^+ + c^- - 2C\right)\boldsymbol{I} - \boldsymbol{\tau_M} \,, \tag{4}$$

given by the difference between the Donnan osmotic pressure (relative to the bulk counterpart P_w) and the Maxwell tensor

$$\boldsymbol{\tau_M} = \frac{\widetilde{\widetilde{\varepsilon\varepsilon}}_0}{2}\left(2\boldsymbol{E}\otimes\boldsymbol{E} - E^2\boldsymbol{I}\right) \,, \tag{5}$$

where $\widetilde{\varepsilon}$ and $\widetilde{\varepsilon}_0$ denote the permittivity of the vacuum and dielectric constant of the water solvent, $\boldsymbol{E} := -\boldsymbol{\nabla}_z\varphi$ is the electric field with φ the double layer electric potential (with reference value $\varphi = 0$ in the bulk fluid). The concentrations of the cations and the anions obey a Boltzmann-type distribution

$$c^{\pm} = C\exp(\mp\frac{F\varphi}{RT})\,, \tag{6}$$

with F and R the Faraday and ideal gas constants and T the temperature. The electric double layer potential φ satisfies the local Poisson-Boltzmann problem

$$\left\{\begin{array}{lcll} \Delta_{zz}\varphi & = & \dfrac{2FC}{\widetilde{\varepsilon}\widetilde{\varepsilon}_0}\sinh\left(\dfrac{F\varphi}{RT}\right) & \text{in} \quad Z_l \\ \boldsymbol{\nabla}_z\varphi\cdot\boldsymbol{n} & = & \dfrac{\sigma}{\widetilde{\varepsilon}\widetilde{\varepsilon}_0} & \text{on} \quad \partial Z_{ls} \end{array}\right. , \tag{7}$$

with $\sigma < 0$ the surface charge density of the particles, ∂Z_{ls} the interface between fluid and solid subdomains and $\boldsymbol{n}$ the unit normal exterior to Z_l.

The contribution of the solid phase to the swelling tensor $\boldsymbol{\Pi}$ consists of the average of the stress tensor σ_Π which satisfies a local elasticity problem in the periodic solid phase with traction vector on the fluid-solid interface induced by the disjoining pressure $\boldsymbol{\Pi}_d$. Thus, denoting $\boldsymbol{u}_\Pi$ the electrochemical component of solid displacement $\boldsymbol{u}$, if the solid phase is assumed incompressible, we have

$$\left\{\begin{array}{lll} \boldsymbol{\nabla}_z\cdot\boldsymbol{\sigma}_\Pi = 0 & & \\ \boldsymbol{\sigma}_\Pi = -p_\Pi\boldsymbol{I} + 2\mu_s^p\boldsymbol{\mathcal{E}}_z(\boldsymbol{u}_\Pi) & & \\ \boldsymbol{\nabla}_z\cdot\boldsymbol{u}_\Pi = 0 & \text{in} \quad Z_s & \\ \boldsymbol{\sigma}_\Pi\boldsymbol{n} = -\boldsymbol{\Pi}_d\boldsymbol{n} & \text{on} \quad \partial Z_{ls}\,. & \end{array}\right. \tag{8}$$

where $p_\pi := -1/3tr(\boldsymbol{\sigma}_\Pi)$ is the pressure in the solid phase and $2\mu_s^p\boldsymbol{\mathcal{E}}_z(\boldsymbol{u}) := \mu_s^p(\boldsymbol{\nabla}_z\boldsymbol{u} + (\boldsymbol{\nabla}_z\boldsymbol{u})^T)$ the deviatoric part of $\boldsymbol{\sigma}_s$ with μ_s^p the shear modulus.

In the case of a stratified nanostructure with geometry characterized by infinite parallel particles of face-to-face contact (Moyne and Murad, 2003; Murad and Moyne, 2008), the disjoining pressure reduces to its component perpendicular to the particle ($\Pi_d = \boldsymbol{\Pi}_d\,\boldsymbol{n}\cdot\boldsymbol{n}$) with Π_d constant given by (Moyne and Murad, 2006b)

$$\Pi_d = 2RTC(\cosh\bar{\varphi}_0 - 1)\,, \tag{9}$$

where $\overline{\varphi}_0$ denotes the dimensionless electric potential in the middle of the interlayer spacing of thickness $2H$ given by $\overline{\varphi}_0 = \overline{\varphi}_0(C,H)$ or $\overline{\varphi}_0 = \overline{\varphi}_0(C,\phi)$ with ϕ the intra-cluster porosity which in the stratified arrangement is given by $\phi = H/(H+\delta)$ with 2δ the clay particle thickness.

For the isotropic microstructure composed of spherical clusters with radially aligned particles within each cluster depicted in Fig. 4, the swelling stress tensor reduces to the

spherical form with a single averaged disjoining pressure component appearing in the main diagonal

$$\boldsymbol{\Pi} := \Pi\, \boldsymbol{I} = \langle \Pi_d \rangle^l \boldsymbol{I}\,. \tag{10}$$

For the sake of simplicity, for radial arrangement of nearly parallel plane particles within each cluster, neglect small differences in the three diagonal components of the Maxwell stress tensor so that we may adopt the simplified representation $\Pi = \Pi_d$ for each component with Π_d constant given by the solution of the electrical double layer theory (9). In addition the stress state induced in the solid phase by the traction due to Π_d is also spherical with $\boldsymbol{\sigma}_\Pi = -\Pi_d\, \boldsymbol{I}$.

Under the local incompressibility assumption for the solid phase, the mass balance of the clay clusters reads

$$\frac{\partial(1-\phi)}{\partial t} + \boldsymbol{\nabla}_y \cdot \left[(1-\phi)\frac{\partial \boldsymbol{u}}{\partial t}\right] = 0\,, \tag{11}$$

where $\boldsymbol{y}$ denotes the microscopic slow coordinate varying at the clay cluster scale. Neglecting the advection induced by the movement of the solid phase gives

$$\frac{\partial \phi}{\partial t} = (1-\phi)\boldsymbol{\nabla}_y \cdot \frac{\partial \boldsymbol{u}}{\partial t}\,. \tag{12}$$

Hence, considering initially an incompressible response of the clusters $\boldsymbol{\nabla}_y \cdot \boldsymbol{u} = 0$, we obtain after integration

$$(1-\phi) = (1-\overline{\phi}) \exp\left(-\boldsymbol{\nabla}_y \cdot \boldsymbol{u}\right), \tag{13}$$

with $\overline{\phi} = \phi(t=0)$ the initial intra-cluster porosity. The overall equilibrium (1) along with the modified effective stress principle (2) and the mass balance of the solid phase (13) supplemented by the closure problem (10) with $\boldsymbol{\Pi} = \Pi_d\, \boldsymbol{I}$ for spherical clay clusters with parallel particle arrangement constitutes our two-scale model for the poromechanics.

3 Coupled microscopic model for clay clusters and micropores

We now pursue the up-scaling process from the micro- to the macroscale by incorporating an additional microporosity level partially saturated with bulk water and air. To this end we begin by establishing the coupled model at the microscale for the clusters and micropores omitting the indices relative to the spatial derivatives for the sake of generality. For the homogenization procedure in the subsequent section the indices relative to the microscopic $\boldsymbol{y}$ and macroscopic variables $\boldsymbol{x}$ will be reintroduced. By revisiting the microscopic geometry depicted in Fig. 2, the expansive medium is represented by a biphasic assembly

of swollen clay clusters and micropores occupying the domains Ω_y^s and Ω_y^f respectively. The mechanics in Ω_y^s is described by the aforementioned two-scale model.

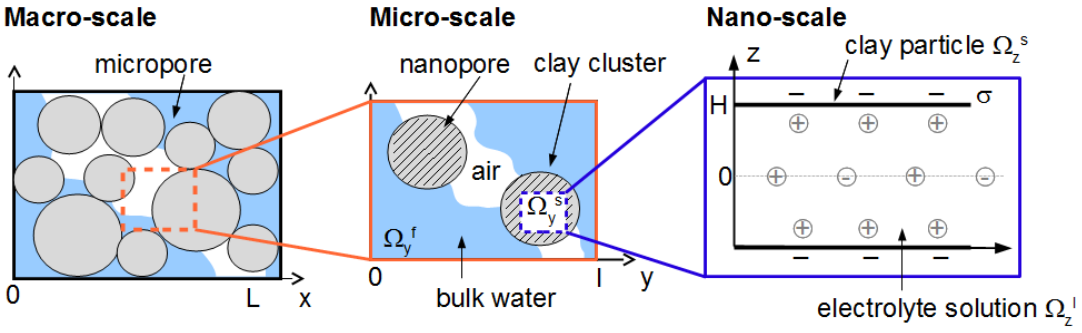

Figure 2: Three-scale representation of the microstructure of a swelling clay.

The micropore domain Ω_y^f is filled with a mixture of air at constant pressure P_a and saline bulk water composed by the same fully dissociated 1:1 electrolytes with given bulk concentrations $C^- = C^+ = C$. The characteristic length scale of the coarser micropores is assumed to be large compared to the Debye length of the EDL, so that the bulk water is free of EDL effects. The time-scale associated with non-equilibrium phenomena is assumed very fast such that the system is at local thermodynamic equilibrium undergoing a quasistatic sequence of equilibrium states with equality between the electrochemical potentials of the ions in the electrolyte solution and bulk water. As we aim at analyzing the competition between disjoining stresses resulting from the nanopore level and capillary effects in the micropores, our development is limited to high saturation levels where the meniscus of the air/water interface is larger than the nanopore diameter so that the bulk water phase in the micropores is assumed continuous. In this scenario capillarity dominates the adsorption of water in the micropores and the matric suction coincides with the capillary pressure.

To establish the proper equilibrium condition for the bulk fluid mixture occupying the domain Ω_y^f we begin by invoking the equivalent pore pressure concept (Coussy and Dangla, 2002; Loret and Khalili, 2002; Pereira *et al.*, 2005; Dormieux *et al.*, 2006; Nikooee *et al.*, 2013). Following Coussy and Dangla (Coussy and Dangla, 2002) within the framework of thermodynamics introduce U as the variation of the free energy of the bulk water/air interface with reference to the fully saturated case per unit of pore volume given by the area underneath the capillary pressure curve (Leverett, 1941; Coussy and Dangla, 2002; Grant and Gerhard, 2007; Nikooee *et al.*, 2013)

$$U(S_w) = \int_{S_w}^{1} P_c(s_w) ds_w \,, \tag{14}$$

Since P_a is constant and $P_c(S_w) = P_a - P_w(S_w)$ we have

$$S_w = P_c^{-1}(P_w)\,. \tag{15}$$

Using (14) the equilibrium equivalent pore pressure of the bulk fluid mixture P_f is introduced as (Coussy and Dangla, 2002; Pereira *et al.*, 2005; Nikooee *et al.*, 2013)

$$P_f = S_a P_a + S_w P_w - kU = S_a P_a + S_w P_w - k\int_{S_w}^{1} P_c(s_w)ds_w\,, \tag{16}$$

with $S_a = 1 - S_w$ denoting the air saturation and k is a factor depending on the constitutive law of U (Coussy and Dangla, 2002; Nikooee *et al.*, 2013). By invoking Hill's lemma (Chateau and Dormieux, 1995) and adopting a macroscopic point of view where U depends on the solid deformation in addition to saturation $U = U(\boldsymbol{\mathcal{E}}(\boldsymbol{u}), S_w)$, Coussy and Dangla (Coussy and Dangla, 2002) showed that for isotropic and reversible contributions of the water/air interfaces $k = 2/3$. Assuming the capillary pressure and thus the interface energy being function of the water saturation only, i.e. $P_c = P_c(S_w)$ and $U = U(S_w)$, Coussy and Dangla derived also values of k for irreversible capillary phenomena. Considering a particular form of microstructure composed of spherical pores of increasing radius interconnected by capillary tubes of negligible volume and for a perfectly wetting liquid, they obtained for imbibition $k^{imb} = 3/2$ (Coussy and Dangla, 2002). For the sake of simplicity, under reversibility in the water retention curve $k = 1$ (Coussy and Dangla, 2002). Under these conditions, P_f in (16) can be expressed as

$$P_f = (1-\chi)P_a + \chi P_w = P_a - \chi P_c\,, \tag{17}$$

where χ denotes the microscopic Bishop parameter defined according to Pereira et al. (Pereira *et al.*, 2005) in the form

$$\chi(S_w) = \begin{cases} 1 & \text{for} \quad P_c \le P_c^e \\ S_w + \dfrac{\int_{S_w}^{1} P_c(s_w)ds_w}{P_c(S_w)} & \text{for} \quad P_c > P_c^e\,, \end{cases} \tag{18}$$

with P_c^e designating the air entry capillary pressure. Under the current assumptions an important feature underlaying the above closure relation is the explicit contribution of the interfaces incorporated in the second term of the rhs resulting in the deviation of χ from S_w. In the absence of such interfacial contribution the equivalent pore pressure defined in (17) reduces to the weighted averaged value $P_f = (1 - S_w)P_a + S_w P_w$ which does not fulfill equilibrium (Coussy and Dangla, 2002; Dormieux *et al.*, 2006).

Denoting $\boldsymbol{\sigma}_f = -P_f \boldsymbol{I}$ the stress tensor of the bulk solution, with P_f defined in (17), the equilibrium of the bulk water air mixture is given by

$$\boldsymbol{\nabla}\cdot\boldsymbol{\sigma}_f + \rho_f \boldsymbol{g} = -\boldsymbol{\nabla}P_f + \rho_f \boldsymbol{g} = 0\,, \tag{19}$$

with $\rho_f := S_w\rho_w + (1 - S_w)\rho_a$ the averaged weighted fluid density. Since $\rho_a << \rho_w$, without loss of generality assume $\rho_f \approx S_w\rho_w$. To summarize, our set of coupled microscopic equations reads

$$\begin{cases} \boldsymbol{\nabla \cdot \sigma}_t + \rho_t \boldsymbol{g} = 0 \\ \boldsymbol{\sigma}_t = -P_w \boldsymbol{I} + \boldsymbol{\sigma}_{el} - \boldsymbol{\Pi} \\ \boldsymbol{\sigma}_{el} = \boldsymbol{C\mathcal{E}}(\boldsymbol{u}) \qquad\qquad \text{in} \quad \Omega_y^s \\ \rho_t = \phi\rho_w + (1-\phi)\rho_s \\ (1-\phi) = (1-\overline{\phi}) \exp\left(-\boldsymbol{\nabla \cdot u}\right) \end{cases}$$

$$\begin{cases} \boldsymbol{\nabla \cdot \sigma}_f + \rho_f \boldsymbol{g} = 0 \\ \boldsymbol{\sigma}_f = -P_f \boldsymbol{I} = -(P_a - \chi P_c)\boldsymbol{I} = -\left[(1-\chi)P_a + \chi P_w\right]\boldsymbol{I} \\ \chi(S_w) = S_w + \dfrac{\int_{S_w}^1 P_c(s_w)ds_w}{P_c(S_w)} \qquad\qquad \text{in} \quad \Omega_y^f\,, \\ \rho_f \approx S_w\rho_w \\ P_c(S_w) = P_a - P_w(S_w) \end{cases} \tag{20}$$

The microscopic equations are supplemented by boundary conditions at the cluster/micropore interface Γ_{fs}. Denoting $\boldsymbol{N}$ the unit normal exterior to Ω_y^s, continuity of the normal component of the overall stress reads

$$\boldsymbol{\sigma}_f \boldsymbol{N} = \boldsymbol{\sigma}_t \boldsymbol{N} \quad \text{on} \qquad \Gamma_{fs}\,. \tag{21}$$

Finally, assuming initially absence of any solid deformation and any capillary and electrochemical efforts, the initial conditions are given by

$$\boldsymbol{\nabla \cdot u} = 0, \qquad S_w = 1, \qquad \phi = \overline{\phi}, \qquad C = \bar{C} \quad \text{such that} \quad \boldsymbol{\Pi}(\overline{\phi}, \overline{C}) = 0, \quad t = 0\,. \tag{22}$$

4 Homogenization

The up-scaling of the microscopic problem to the macroscale is accomplished using the homogenization method of periodic structures (Auriault *et al.*, 2009; Sanchez-Palencia, 1980). Within this framework two separate length scales are introduced: a microscopic scale l of the size of a clay cluster and a macroscopic scale L of the overall dimension of the porous medium. Their ratio $\epsilon = l/L << 1$ is the small perturbation parameter under the scale-separation assumption. The swelling medium Ω^ϵ is idealized as a bounded domain composed of spatially repeated parallelepiped cells Q^ϵ at the microscale (Fig. 3). Likewise, the cluster and micropore subdomains Ω_s^ϵ and Ω_f^ϵ together with their common interface Γ_{fs}^ϵ are given by the union of the cell domains Q_s^ϵ and Q_f^ϵ along with the interface ∂Q_{fs}^ϵ. Each cell Q^ϵ is congruent to a standard Q composed of reference subdomains Q_f and Q_s representing the micropores and swollen clay clusters with interface ∂Q_{fs}. After scaling

properly the microscopic model in terms of ϵ our aim is to investigate the asymptotic solution as $\epsilon \to 0$ and obtain the homogenized limit as the scale of the inhomogeneity tends to zero.

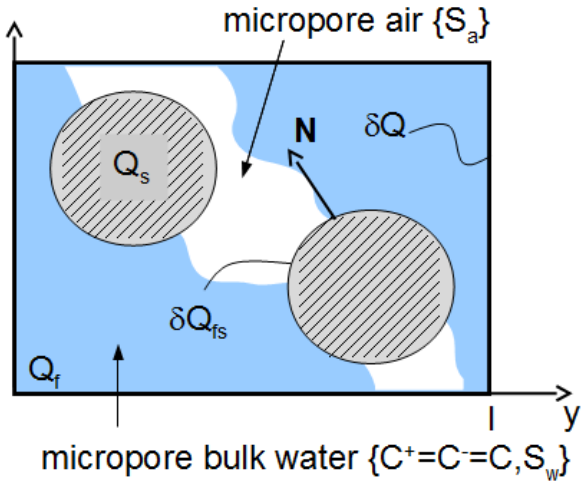

Figure 3: Microscopic periodic cell Q composed of the subdomains occupied by the swollen clay clusters Q_s and micropores Q_f.

4.1 Asymptotic expansions

Within the framework of homogenization each property ν^ϵ depends on global and local length scales represented in terms of the slow $\boldsymbol{x}$ and the fast $\boldsymbol{y} = \boldsymbol{x}/\epsilon$ coordinates. Then, postulate the asymptotic expansion

$$\nu^\epsilon = \sum_{k=0}^{\infty} \epsilon^k \nu^k \,, \tag{23}$$

with the coefficients ν^k, Q-periodic in $\boldsymbol{y}$. The above ansatz is introduced in the microscopic model with the differential operator $\boldsymbol{\nabla}$ replaced by $\boldsymbol{\nabla}_x + 1/\epsilon \boldsymbol{\nabla}_y$. The formal matching of the different powers of ϵ allows to obtain an hierarchy of problems ruled by the successive $\mathcal{O}(\epsilon)$.

In addition, we make use of the integral form of the time- and space-averaging theorems to compute the porosity of the micropores. Let f^ϵ and $\boldsymbol{g}^\epsilon$ be general scalar and vectorial functions defined in Ω_i^ϵ $(i = f, s)$ and denote the velocity of the clay cluster/micropore interface by $\partial \boldsymbol{u}^\epsilon / \partial t$. The ratio between volume and area of the periodic cell scales with $\mathcal{O}(\epsilon^3)/\mathcal{O}(\epsilon^2)$ and thus we adopt the scaling $|Q^\epsilon| / |\partial Q_{fs}^\epsilon| = \mathcal{O}(\epsilon)$. The rescaled form of the time- and space-averaging theorems in Q_f, with the averaging operator given by

$\langle\cdot\rangle = |Q|^{-1}\int_{Q_f}\cdot\, dQ$, reads as (remind that $\boldsymbol{N}$ was chosen outwards to Q_s) (Moyne and Murad, 2006a)

$$\begin{aligned}\left\langle\frac{\partial f^\epsilon}{\partial t}\right\rangle &= \frac{\partial\langle f^\epsilon\rangle}{\partial t} + \frac{1}{|\epsilon Q|}\int_{\partial Q_{fs}} f^\epsilon\frac{\partial \boldsymbol{u}^\epsilon}{\partial t}\cdot\boldsymbol{N}\ \mathrm{d}\Gamma\\ \langle\boldsymbol{\nabla}\cdot\boldsymbol{g}^\epsilon\rangle &= \boldsymbol{\nabla}\cdot\langle\boldsymbol{g}^\epsilon\rangle - \frac{1}{|\epsilon Q|}\int_{\partial Q_{fs}}\boldsymbol{g}^\epsilon\cdot\boldsymbol{N}\ \mathrm{d}\Gamma\,,\end{aligned} \tag{24}$$

which at $\mathcal{O}(\epsilon^0)$ gives

$$\left\langle\frac{\partial f^0}{\partial t}\right\rangle = \frac{\partial\langle f^0\rangle}{\partial t} + \frac{1}{|Q|}\int_{\partial Q_{fs}}\left(f\frac{\partial \boldsymbol{u}}{\partial t}\right)^1\cdot\boldsymbol{N}\ \mathrm{d}\Gamma \tag{25}$$

$$\left\langle\boldsymbol{\nabla}_x\cdot\boldsymbol{g}^0 + \boldsymbol{\nabla}_y\cdot\boldsymbol{g}^1\right\rangle = \boldsymbol{\nabla}_x\cdot\left\langle\boldsymbol{g}^0\right\rangle - \frac{1}{|Q|}\int_{\partial Q_{fs}}\boldsymbol{g}^1\cdot\boldsymbol{N}\ \mathrm{d}\Gamma\,. \tag{26}$$

By setting $\boldsymbol{g}^\epsilon = f^\epsilon\partial\boldsymbol{u}^\epsilon/\partial t$, so that $\boldsymbol{g}^0 = f^0\partial\boldsymbol{u}^0/\partial t$ and $\boldsymbol{g}^1 = (f\partial\boldsymbol{u}/\partial t)^1$, we have after adding (25) and (26)

$$\left\langle\frac{\partial f^0}{\partial t}\right\rangle + \left\langle\boldsymbol{\nabla}_x\cdot\left(f^0\frac{\partial\boldsymbol{u}^0}{\partial t}\right)\right\rangle + \left\langle\boldsymbol{\nabla}_y\cdot\left(f^0\frac{\partial\boldsymbol{u}^1}{\partial t} + f^1\frac{\partial\boldsymbol{u}^0}{\partial t}\right)\right\rangle = \frac{\partial\langle f^0\rangle}{\partial t} + \boldsymbol{\nabla}_x\cdot\left\langle f^0\frac{\partial\boldsymbol{u}^0}{\partial t}\right\rangle. \tag{27}$$

The different orders of the governing equations in the micropore domain Q_f are given by

$$\boldsymbol{\nabla}_y\cdot\boldsymbol{\sigma}_f^0 = 0 \tag{28}$$

$$\boldsymbol{\nabla}_x\cdot\boldsymbol{\sigma}_f^0 + \boldsymbol{\nabla}_y\cdot\boldsymbol{\sigma}_f^1 + \rho_f^0\boldsymbol{g} = 0 \tag{29}$$

$$\boldsymbol{\sigma}_f^0 = -P_f^0\boldsymbol{I} = -\left(P_a - \chi^0 P_c^0\right)\boldsymbol{I} = -\left[(1-\chi^0)P_a + \chi^0 P_w^0\right]\boldsymbol{I} \tag{30}$$

$$\boldsymbol{\sigma}_f^1 = -P_f^1\boldsymbol{I} \tag{31}$$

$$\chi^0(S_w^0) = S_w^0 + \frac{\int_{S_w^0}^1 P_c^0(s_w^0)ds_w^0}{P_c^0(S_w^0)} \tag{32}$$

$$\rho_f^0 = S_w^0\rho_w \tag{33}$$

$$P_c^0(S_w^0) = P_a - P_w^0(S_w^0)\,, \tag{34}$$

whereas the mechanical model in Q_s at successive orders is given by

$$\boldsymbol{\sigma}_t^0 = -P_w^0 \boldsymbol{I} + \boldsymbol{\sigma}_{el}^0 - \boldsymbol{\Pi}^0 \tag{35}$$
$$\boldsymbol{\sigma}_{el}^0 = \boldsymbol{C}\left[\boldsymbol{\mathcal{E}}_x(\boldsymbol{u}^0) + \boldsymbol{\mathcal{E}}_y(\boldsymbol{u}^1)\right] \tag{36}$$
$$\boldsymbol{\nabla}_y \cdot \left[\boldsymbol{C}\boldsymbol{\mathcal{E}}_y(\boldsymbol{u}^0)\right] = 0 \tag{37}$$
$$\boldsymbol{\nabla}_x \cdot \left[\boldsymbol{C}\boldsymbol{\mathcal{E}}_y(\boldsymbol{u}^0)\right] + \boldsymbol{\nabla}_y \cdot \boldsymbol{\sigma}_t^0 = 0 \tag{38}$$
$$\boldsymbol{\nabla}_x \cdot \boldsymbol{\sigma}_t^0 + \boldsymbol{\nabla}_y \cdot \boldsymbol{\sigma}_t^1 + \rho_t^0 \boldsymbol{g} = 0 \tag{39}$$
$$\rho_t^0 = \phi^0 \rho_w + (1-\phi^0)\rho_s \tag{40}$$
$$(1-\phi^0) = (1-\overline{\phi})\exp\left(-\boldsymbol{\nabla}_x \cdot \boldsymbol{u}^0 - \boldsymbol{\nabla}_y \cdot \boldsymbol{u}^1\right). \tag{41}$$

The different orders of the boundary conditions on ∂Q_{fs} are

$$\boldsymbol{C}\boldsymbol{\mathcal{E}}_y(\boldsymbol{u}^0)\boldsymbol{N} = 0 \tag{42}$$
$$\boldsymbol{\sigma}_t^0 \boldsymbol{N} = \boldsymbol{\sigma}_f^0 \boldsymbol{N} \tag{43}$$
$$\boldsymbol{\sigma}_t^1 \boldsymbol{N} = \boldsymbol{\sigma}_f^1 \boldsymbol{N}. \tag{44}$$

Finally, the $\mathcal{O}(\epsilon^0)$ of the initial conditions is given by

$$\boldsymbol{\nabla}_x \cdot \boldsymbol{u}^0 = \boldsymbol{\nabla}_y \cdot \boldsymbol{u}^1 = 0, \qquad S_w^0 = 1, \qquad \phi^0 = \overline{\phi}, \qquad C^0 = \overline{C}, \quad \text{at} \quad t = 0. \tag{45}$$

4.2 Non-oscillatory variables

From (28) and (30) it follows that $P_f^0 = P_f^0(\boldsymbol{x})$. In addition using (34), (32) and (33), we have $P_w^0 = P_w^0(\boldsymbol{x})$, $S_w^0 = S_w^0(\boldsymbol{x})$, $P_c^0 = P_c^0(\boldsymbol{x})$, $\chi^0 = \chi^0(\boldsymbol{x})$ and $\rho_f^0 = \rho_f^0(\boldsymbol{x})$. The microscopic closure problem for $P_f^1(\boldsymbol{x}, \boldsymbol{y})$ is obtained from (29) and (31)

$$\boldsymbol{\nabla}_x P_f^0 + \boldsymbol{\nabla}_y P_f^1 - \rho_f^0 \boldsymbol{g} = 0. \tag{46}$$

Hence, integrating furnishes the linear dependency

$$P_f^1(\boldsymbol{x}, \boldsymbol{y}) = (-\boldsymbol{\nabla}_x P_f^0 + \rho_f^0 \boldsymbol{g}) \cdot \boldsymbol{y} + \bar{P}_f^1(\boldsymbol{x}). \tag{47}$$

On the other hand, the enforcement of periodic boundary conditions precludes the dependence $P_f^1 = P_f^1(\boldsymbol{y})$ which implies

$$\boldsymbol{\nabla}_x P_f^0 = \rho_f^0 \boldsymbol{g} \quad \rightarrow \quad P_f^0(\boldsymbol{x}) = \rho_f^0 \boldsymbol{g} \cdot \boldsymbol{x} + \bar{P}_f^0, \tag{48}$$

where $\bar{P}_f^0$ is a constant and $\boldsymbol{\nabla}_x P_f^0 = \chi^0 \boldsymbol{\nabla}_x P_w^0 + (P_w^0 - P_a)\boldsymbol{\nabla}_x \chi^0 = \chi^0 \boldsymbol{\nabla}_x P_w^0 - P_c^0 \boldsymbol{\nabla}_x \chi^0$. A crucial variable in our development which incorporates the coupling between capillary

effects and the mechanics of the clay clusters is the pressure excess γ^0 of the bulk mixture relative to the water pressure in the nanopores

$$\begin{aligned}\gamma^0\left(S_w^0(\boldsymbol{x})\right) &:= P_f^0 - P_w^0 \\ &= \chi^0 P_w^0 + (1-\chi^0)P_a - P_w^0 \\ &= (1-\chi^0)(P_a - P_w^0) \\ &= (1-\chi^0)P_c^0\,. \end{aligned} \tag{49}$$

Finally $\boldsymbol{u}^0$ is defined by the Neumann problem (37) and (42) whose solution is the rigid motion $\boldsymbol{u}^0 = \boldsymbol{u}^0(\boldsymbol{x})$. Thus, our set of non-oscillatory variables is $\left\{\boldsymbol{u}^0, S_w^0, \chi^0, P_f^0, P_w^0, P_c^0, \gamma^0\right\}$.

4.3 Microscopic closure problem

The local cell problem for the fluctuating displacement $\boldsymbol{u}^1$ is obtained from the elasticity problem at $\mathcal{O}(\epsilon^{-1})$ (38) along with the constitutive laws (35), (36) and the boundary condition (43). We then have, using (30) and (49) for the bulk water

$$\begin{aligned} &\boldsymbol{\nabla}_y \cdot \left[\boldsymbol{C}\boldsymbol{\mathcal{E}}_y(\boldsymbol{u}^1) - \boldsymbol{\Pi}^0\right] = 0 && \text{in} \quad Q_s \\ &\left(\gamma^0\boldsymbol{I} + \boldsymbol{C}\left[\boldsymbol{\mathcal{E}}_x(\boldsymbol{u}^0) + \boldsymbol{\mathcal{E}}_y(\boldsymbol{u}^1)\right] - \boldsymbol{\Pi}^0\right)\boldsymbol{N} = 0 && \text{on} \quad \partial Q_{fs}\,. \end{aligned} \tag{50}$$

The above form of the Neumann problem is similar to its two-scale counterpart (8) within the clay clusters. Indeed it should be noted the reverse sign of $\boldsymbol{\Pi}^0$ compared to $\boldsymbol{\Pi}_d$, which now acts to mitigate swelling due to fluctuation in the $\boldsymbol{y}$-coordinate. The novelty here is the appearance of the excess fluid pressure γ^0 which quantifies the influence of capillary effects upon the fluctuating displacement. In a similar fashion to its two-scale counterpart (Moyne and Murad, 2002) $\boldsymbol{u}^1$ admits the decomposition

$$\boldsymbol{u}^1(\boldsymbol{x},\boldsymbol{y}) = \boldsymbol{\xi}(\boldsymbol{y})\boldsymbol{\mathcal{E}}_x(\boldsymbol{u}^0(\boldsymbol{x})) + \boldsymbol{\eta}(\boldsymbol{y})\gamma^0(\boldsymbol{x}) + \boldsymbol{u}_\Pi^1(\boldsymbol{x},\boldsymbol{y}) + \bar{\boldsymbol{u}}^1(\boldsymbol{x})\,. \tag{51}$$

The canonical cell problems for the third order tensor $\boldsymbol{\xi}$ and the vector $\boldsymbol{\eta}$ are the same of classical poroelasticity (Auriault, 1990)

$$\left\{\begin{array}{ll} \boldsymbol{\nabla}_y \cdot [\boldsymbol{C}\boldsymbol{\mathcal{E}}_y(\boldsymbol{\xi})] = 0 & \text{in} \quad Q_s \\ [\boldsymbol{\mathcal{E}}_y(\boldsymbol{\xi}) + \boldsymbol{I}]\,\boldsymbol{N} = 0 & \text{on} \quad \partial Q_{fs} \end{array}\right. \quad \left\{\begin{array}{ll} \boldsymbol{\nabla}_y \cdot [\boldsymbol{C}\boldsymbol{\mathcal{E}}_y(\boldsymbol{\eta})] = 0 & \text{in} \quad Q_s \\ [\boldsymbol{C}\boldsymbol{\mathcal{E}}_y(\boldsymbol{\eta}) + \boldsymbol{I}]\,\boldsymbol{N} = 0 & \text{on} \quad \partial Q_{fs}\,. \end{array}\right. \tag{52}$$

The local cell problem of the purely expansive component $\boldsymbol{u}_\Pi^1$ reflects swelling mitigation due to the transmissibility of $\boldsymbol{\Pi}^0$ between adjacent clusters

$$\left\{\begin{array}{ll} \boldsymbol{\nabla}_y \cdot \left[\boldsymbol{C}\boldsymbol{\mathcal{E}}_y(\boldsymbol{u}_\Pi^1) - \boldsymbol{\Pi}^0\right] = 0 & \text{in} \quad Q_s \\ \left[\boldsymbol{C}\boldsymbol{\mathcal{E}}_y(\boldsymbol{u}_\Pi^1) - \boldsymbol{\Pi}^0\right]\boldsymbol{N} = 0 & \text{on} \quad \partial Q_{fs}\,. \end{array}\right. \tag{53}$$

An important feature is the mechanical coupling induced by capillarity effects through the excess pressure γ^0 in (50). As we shall illustrate later, the appearance of the different components (elastic, capillary and electrochemical) in the closure problem (51) is crucial to establish the correct form of the macroscopic effective stress principle.

By averaging the constitutive equation (36) for $\boldsymbol{\sigma}_{el}^0$ over the unit cell and using the closure relation (51) we obtain

$$\left\langle \boldsymbol{\sigma}_{el}^0 \right\rangle = \boldsymbol{C}^{eff} \boldsymbol{\mathcal{E}}_x(\boldsymbol{u}^0) + \left\langle \boldsymbol{C}\boldsymbol{\mathcal{E}}_y(\boldsymbol{\eta}) \right\rangle \gamma^0 + \left\langle \boldsymbol{C}\boldsymbol{\mathcal{E}}_y(\boldsymbol{u}_\Pi^1) \right\rangle \,, \tag{54}$$

where the coefficient $\boldsymbol{C}^{eff}$ denotes the macroscopic elasticity tensor

$$\boldsymbol{C}^{eff} = \left\langle \boldsymbol{C}\left(\boldsymbol{II} + \boldsymbol{\mathcal{E}}_y(\boldsymbol{\xi})\right) \right\rangle \,, \tag{55}$$

with $\boldsymbol{II} = \boldsymbol{I} \otimes \boldsymbol{I}$ the unit forth order tensor.

4.4 Modified effective stress principle

To derive the overall equilibrium condition we average (39) and (29) and make use of the boundary condition (44). Recalling that $\boldsymbol{N}$ was chosen outwards to Q_s, this yields

$$\begin{aligned}
\boldsymbol{\nabla}_x \cdot \left\langle \boldsymbol{\sigma}_t^0 \right\rangle + \left\langle \rho_t^0 \right\rangle \boldsymbol{g} &= -\frac{1}{|Q|} \int_{Q_s} \boldsymbol{\nabla}_y \cdot \boldsymbol{\sigma}_t^1 \, dQ \\
&= -\frac{1}{|Q|} \int_{\partial Q_{fs}} \boldsymbol{\sigma}_t^1 \boldsymbol{N} \, d\Gamma = -\frac{1}{|Q|} \int_{\partial Q_{fs}} \boldsymbol{\sigma}_f^1 \boldsymbol{N} \, d\Gamma \\
&= \frac{1}{|Q|} \int_{Q_f} \boldsymbol{\nabla}_y \cdot \boldsymbol{\sigma}_f^1 \, dQ \\
&= -\boldsymbol{\nabla}_x \cdot \left\langle \boldsymbol{\sigma}_f^0 \right\rangle - \left\langle \rho_f^0 \right\rangle \boldsymbol{g} \,.
\end{aligned} \tag{56}$$

Thus, define the total macroscopic stress in the form

$$\boldsymbol{\sigma}_T := \begin{cases} \left\langle \boldsymbol{\sigma}_t^0 \right\rangle & \text{in} \quad Q_s \\ \left\langle \boldsymbol{\sigma}_f^0 \right\rangle & \text{in} \quad Q_f \,, \end{cases} \tag{57}$$

and the mean total density ρ_T by the combination of (33) with (40)

$$\begin{aligned}
\rho_T &:= \left\langle \rho_t^0 \right\rangle + \left\langle \rho_f^0 \right\rangle = n_s \left\langle \rho_t^0 \right\rangle^s + n_f \rho_f^0 \\
&= \left[(1 - n_f) \left\langle \phi^0 \right\rangle^s + n_f S_w^0 \right] \rho_w + (1 - n_f)(1 - \left\langle \phi^0 \right\rangle^s) \rho_s \,,
\end{aligned} \tag{58}$$

where $n_f = |Q_f| \,/\, |Q|$ and $n_s = |Q_s| \,/\, |Q| = 1 - n_f$ denote the macroscopic volume fractions of the micropores and clay clusters respectively and $\langle \cdot \rangle^s := |Q_s|^{-1} \displaystyle\int_{Q_s} \cdot \, \mathrm{d}Q =$

$(1-n_f)^{-1}\langle\cdot\rangle$ the intrinsic volume averaging operator over the solid phase. From (56)-(58) we obtain the macroscopic equilibrium

$$\boldsymbol{\nabla}_x \cdot \boldsymbol{\sigma}_T + \rho_T \boldsymbol{g} = 0 \qquad \text{in} \quad \Omega\,. \tag{59}$$

We then introduce the tensorial generalization of the Biot-Willis coefficient as (Biot and Willis, 1957; Auriault, 1990)

$$\boldsymbol{\alpha} = n_f \boldsymbol{I} - \langle \boldsymbol{C}\boldsymbol{\mathcal{E}}_y(\boldsymbol{\eta})\rangle = n_f \boldsymbol{I} - \langle \boldsymbol{\nabla}_y \cdot \boldsymbol{\xi}\rangle\,, \tag{60}$$

and the macroscopic elastic stress $\boldsymbol{\sigma}_E$ in the form

$$\boldsymbol{\sigma}_E = \boldsymbol{C}^{eff}\boldsymbol{\mathcal{E}}_x(\boldsymbol{u}^0)\,. \tag{61}$$

The above result combined with (30), (35), (49) and (54) provides the following decomposition for the total stress

$$\begin{aligned}
\boldsymbol{\sigma}_T &= \left\langle \boldsymbol{\sigma}_t^0 \right\rangle + \left\langle \boldsymbol{\sigma}_f^0 \right\rangle \\
&= -(1-n_f)P_w^0 \boldsymbol{I} + \left\langle \boldsymbol{\sigma}_{el}^0 \right\rangle - \left\langle \boldsymbol{\Pi}^0 \right\rangle - n_f P_f^0 \boldsymbol{I} \\
&= \boldsymbol{\sigma}_E - \boldsymbol{\alpha}(1-\chi^0)P_a - \left[\boldsymbol{I} - \boldsymbol{\alpha}(1-\chi^0)\right] P_w^0 - \boldsymbol{\Pi}_{eff} \qquad \text{in} \quad \Omega\,,
\end{aligned} \tag{62}$$

where $\boldsymbol{\Pi}_{eff}^0$ designates the three-scale swelling stress tensor

$$\boldsymbol{\Pi}_{eff} = \left\langle \boldsymbol{\Pi}^0 - \boldsymbol{C}\boldsymbol{\mathcal{E}}_y(\boldsymbol{u}_\Pi^1)\right\rangle\,. \tag{63}$$

This closure relation furnishes two components of $\boldsymbol{\Pi}_{eff}$, one resulting from the macroscopic averaging of the swelling stress $\boldsymbol{\Pi}^0$ over the subdomain occupied by the clay clusters and the compressible elastic component $\boldsymbol{\Pi}_s := -\langle \boldsymbol{C}\boldsymbol{\mathcal{E}}_y(\boldsymbol{u}_\Pi^1)\rangle$. As quoted before, such latter component tends to reduce the magnitude of $\boldsymbol{\Pi}_{eff}$ by subtracting the contact stresses from the mean value of the two-scale swelling stress $\left\langle \boldsymbol{\Pi}^0\right\rangle$. It should be noted that the conditions $\boldsymbol{\Pi}_{eff} \neq 0$ is tied-up to the existence of contact area between the clusters so that the two components in (63) do not cancel out.

Eq. (62) is our main result and represents the modified effective stress principle at the macroscale. In what follows we define the three-scale versions of the Bishop parameter and equivalent pore pressure also accounting for the adsorbed water in the nanopores. By pursuing the analogy of (62) with the two-scale relation for the equivalent pore pressure (30) define the effective Bishop parameter in the form

$$\boldsymbol{\chi}^{eff} := \boldsymbol{I} - (1-\chi^0)\boldsymbol{\alpha}\,, \tag{64}$$

so that the effective stress principle (62) can be rephrased in the form

$$\boldsymbol{\sigma}_T = \boldsymbol{\sigma}_E - P_a \boldsymbol{I} + \boldsymbol{\chi}^{eff} P_c^0 - \boldsymbol{\Pi}_{eff}\,. \tag{65}$$

A crucial feature underlaying the above definition is the deviation from the classical Bishop parameter induced by the cluster compressibility governed by the parameter $\boldsymbol{\alpha}$. In particular by denoting $\tilde{K}$ and K_s the bulk modulus of the clay matrix and cluster respectively and recalling the classical relation (Biot and Willis, 1957)

$$\alpha = \frac{1}{3} tr(\boldsymbol{\alpha}) = 1 - \frac{\tilde{K}}{K_s}\,, \tag{66}$$

from (64) and (66) we have for the volumetric part of the tensorial Bishop coefficient

$$\begin{aligned} \chi^{eff} &:= \frac{1}{3} tr(\boldsymbol{\chi}^{eff}) \\ &= 1 - (1 - \chi^0)\left(1 - \frac{\tilde{K}}{K_s}\right) \\ &= \frac{\tilde{K}}{K_s}(1 - \chi^0) + \chi^0\,. \end{aligned} \tag{67}$$

The above result shows that the effect of cluster compressibility tied-up to the drainage of the adsorbed water $\tilde{K}/K_s$ tends to increase χ^{eff} compared to its two-scale counterpart χ^0. In a similar fashion to (17) an effective equivalent pore pressure tensor $\boldsymbol{P}_f^{eff}$ can be defined as

$$\boldsymbol{P}_f^{eff} = (\boldsymbol{I} - \boldsymbol{\chi}^{eff}) P_a + \boldsymbol{\chi}^{eff} P_w^0 = P_a \boldsymbol{I} - \boldsymbol{\chi}^{eff} P_c\,, \tag{68}$$

which allows to rephrase (65) in terms of $\boldsymbol{P}_f^{eff}$ in the form

$$\boldsymbol{\sigma}_T = \boldsymbol{\sigma}_E - \boldsymbol{P}_f^{eff} - \boldsymbol{\Pi}_{eff} \qquad \text{in} \quad \Omega\,. \tag{69}$$

It should be noted that given $P_c^0 = P_c^0(S_w^0)$, Eq. (18), (64) and (68) can be explored to construct constitutive laws for $\boldsymbol{\chi}^{eff}$ and $\boldsymbol{P}_f^{eff}$.

4.5 Intra- and inter-cluster porosities

To complete the macroscopic description, we need to derive expressions for the inter- and intra-cluster porosities. To this end we make use of the time-averaging theorem (25) choosing f equal to the indicator function $\upsilon(\boldsymbol{y})$

$$\upsilon(\boldsymbol{y}) = \begin{cases} 0 & \text{for} \quad \boldsymbol{y} \in Q_s \\ 1 & \text{for} \quad \boldsymbol{y} \in Q_f\,. \end{cases} \tag{70}$$

For the choice, we have $f^0 = \upsilon$, $f^1 = 0$ and $\langle f^0 \rangle = n_f$ so that combination with the closure relation for the fluctuating displacement (51) gives

$$\frac{\partial n_f}{\partial t} = -\frac{1}{|Q|}\int_{\partial Q_{fs}} \frac{\partial \boldsymbol{u}^1}{\partial t}\cdot \boldsymbol{N}\, d\Gamma = -\frac{1}{|Q|}\int_{Q_s} \boldsymbol{\nabla}_y \cdot \frac{\partial \boldsymbol{u}^1}{\partial t}\, dQ = -\left\langle \boldsymbol{\nabla}_y \cdot \frac{\partial \boldsymbol{u}^1}{\partial t}\right\rangle$$
$$= -\left\langle \boldsymbol{\nabla}_y \cdot \boldsymbol{\xi}\, \frac{\partial \boldsymbol{\mathcal{E}}_x(\boldsymbol{u}^0)}{\partial t} + \boldsymbol{\nabla}_y \cdot \boldsymbol{\eta}\, \frac{\partial \gamma^0}{\partial t} + \boldsymbol{\nabla}_y \cdot \frac{\partial \boldsymbol{u}^1_{\Pi}}{\partial t}\right\rangle \qquad \text{in} \quad \Omega\,. \tag{71}$$

Hence, by invoking the initial condition (45) and definition (49), the above relation yields after integration

$$n_f = \bar{n}_f - \langle \boldsymbol{\nabla}_y \cdot \boldsymbol{\xi}\rangle\, \boldsymbol{\mathcal{E}}_x(\boldsymbol{u}^0) - \langle \boldsymbol{\nabla}_y \cdot \boldsymbol{\eta}\rangle\, (1-\chi^0) P_c^0 - \left\langle \boldsymbol{\nabla}_y \cdot \boldsymbol{u}^1_{\Pi}\right\rangle\,, \tag{72}$$

where $\bar{n}_f$ denotes the value of the initial inter-cluster porosity. For the derivation of the governing equation for the intra-cluster porosity we write the mass balance of the clay clusters (11) at $\mathcal{O}(\epsilon^0)$

$$\frac{\partial(1-\phi^0)}{\partial t} + \boldsymbol{\nabla}_x \cdot \left[(1-\phi^0)\frac{\partial \boldsymbol{u}^0}{\partial t}\right] + \boldsymbol{\nabla}_y \cdot \left[(1-\phi)\frac{\partial \boldsymbol{u}}{\partial t}\right]^1 = 0\,. \tag{73}$$

The intra-cluster porosity is obtained by averaging the above equation in combination with (27) by setting $f = 1-\phi$ so that $f^0 = 1-\phi^0$. This yields

$$\frac{\partial \langle 1-\phi^0\rangle}{\partial t} = -\boldsymbol{\nabla}_x \cdot \left\langle (1-\phi^0)\frac{\partial \boldsymbol{u}^0}{\partial t}\right\rangle\,. \tag{74}$$

Hence, neglecting advection induced by the solid motion gives

$$\frac{1}{\langle 1-\phi^0\rangle}\frac{\partial \langle 1-\phi^0\rangle}{\partial t} = -\boldsymbol{\nabla}_x \cdot \frac{\partial \boldsymbol{u}^0}{\partial t}\,, \tag{75}$$

which furnishes using the initial data in (45)

$$(1-n_f)(1-\left\langle \phi^0\right\rangle^s) = (1-\bar{n}_f)(1-\left\langle \overline{\phi}\right\rangle^s)\exp\left[-\boldsymbol{\nabla}_x \cdot \boldsymbol{u}^0\right]\,. \tag{76}$$

4.6 Summary of the three-scale model of unsaturated expansive clays

Let Ω_M be the macroscopic domain occupied by the swelling clay soil. The formal homogenization procedure of the microscopic model gives rise to the following three-scale model: given C and S_w^0 find the macroscopic unknowns $\left\{\boldsymbol{\sigma}_T, \boldsymbol{\sigma}_E, \boldsymbol{u}^0, \boldsymbol{P}_f^{eff}, P_c^0, P_w^0, \rho_T, n_f, \langle\phi^0\rangle^s\right\}$ functions of $(\boldsymbol{x}, t)$ such that

$$\left\{\begin{array}{l}
\boldsymbol{\nabla}_x \cdot \boldsymbol{\sigma}_T + \rho_T \boldsymbol{g} = 0 \\
\boldsymbol{\sigma}_T = \boldsymbol{\sigma}_E - \boldsymbol{P}_f^{eff} - \boldsymbol{\Pi}_{eff} \\
\boldsymbol{\sigma}_E = \boldsymbol{C}^{eff} \boldsymbol{\mathcal{E}}_x(\boldsymbol{u}^0) \\
\boldsymbol{P}_f^{eff} = P_a \boldsymbol{I} - \boldsymbol{\chi}^{eff} P_c^0 \\
\chi^0 \boldsymbol{\nabla}_x P_w^0 - P_c^0 \boldsymbol{\nabla}_x \chi^0 = \rho_w S_w^0 \boldsymbol{g} \\
P_c^0(S_w^0) = P_a - P_w^0(S_w^0) \\
\rho_T = \left[(1-n_f)\left\langle \phi^0 \right\rangle^s + n_f S_w^0\right] \rho_w + (1-n_f)(1-\left\langle \phi^0 \right\rangle^s)\rho_s \\
n_f = \bar{n}_f - \langle \boldsymbol{\nabla}_y \cdot \boldsymbol{\xi} \rangle \boldsymbol{\mathcal{E}}_x(\boldsymbol{u}^0) - \langle \boldsymbol{\nabla}_y \cdot \boldsymbol{\eta} \rangle (1-\chi^0) P_c^0 - \langle \boldsymbol{\nabla}_y \cdot \boldsymbol{u}_\Pi^1 \rangle \\
(1-\left\langle \phi^0 \right\rangle^s)(1-n_f) = (1-\left\langle \overline{\phi} \right\rangle^s)(1-\bar{n}_f) \exp\left[-\boldsymbol{\nabla}_x \cdot \boldsymbol{u}^0\right]
\end{array}\right. \quad \text{in} \quad \Omega_M\,, \tag{77}$$

where the macroscopic parameters are given by

$$\left\{\begin{array}{l}
\boldsymbol{C}^{eff} = \langle \boldsymbol{C}\,(\boldsymbol{I}\boldsymbol{I} + \boldsymbol{\mathcal{E}}_y(\boldsymbol{\xi})) \rangle \\
\boldsymbol{\alpha} = n_f \boldsymbol{I} - \langle \boldsymbol{C} \boldsymbol{\mathcal{E}}_y(\boldsymbol{\eta}) \rangle \\
\boldsymbol{\chi}^{eff} = \boldsymbol{I} - (1-\chi^0)\boldsymbol{\alpha} \\
\boldsymbol{\Pi}_{eff} = \left\langle \boldsymbol{\Pi}^0 - \boldsymbol{C} \boldsymbol{\mathcal{E}}_y(\boldsymbol{u}_\Pi^1) \right\rangle
\end{array}\right. \tag{78}$$

with χ^0 determined by (32), the characteristic functions $(\boldsymbol{\xi}, \boldsymbol{\eta})$ by (52) and $\boldsymbol{u}_\Pi^1$ computed through (53), where $\boldsymbol{\Pi}^0 \approx \Pi_d \boldsymbol{I}$ for nearly parallel particle arrangement with Π_d given by (9) and the local EDL potential φ^0 solution of the local Poisson-Boltzmann problem.

4.7 Three-scale model of unsaturated expansive clays in the context of conjugated state variables

The modified effective stress principle (65) along with the constitutive laws for P_c^0 and $\boldsymbol{\Pi}^{eff}$ can be rephrased in terms of work-conjugated state variables in the form

$$\left(\begin{array}{l}
\boldsymbol{\sigma}_E = \boldsymbol{C}^{eff} \boldsymbol{\mathcal{E}}_x(\boldsymbol{u}^0) = \boldsymbol{\sigma}_T + P_a \boldsymbol{I} - \boldsymbol{\chi}^{eff} P_c^0 \boldsymbol{I} + \boldsymbol{\Pi}_{eff} \\
P_c^0 = P_a - P_w^0 \\
\boldsymbol{\Pi}_{eff} = \left\langle \boldsymbol{\Pi}^0 - \boldsymbol{C} \boldsymbol{\mathcal{E}}_y(\boldsymbol{u}_\Pi^1) \right\rangle
\end{array}\right) \Leftrightarrow \left(\begin{array}{l}
\boldsymbol{\mathcal{E}}_x(\boldsymbol{u}^0) \\
S_w^0 \\
C
\end{array}\right), \tag{79}$$

The above thermodynamic formulation can be envisioned as a generalization of the well-known two sets of state variables due to the appearance of the additional nanopore level fully saturated by the aqueous electrolyte solution. The classical set of coupled elastic stress $\boldsymbol{\sigma}_E$/macroscopic strain $\boldsymbol{\mathcal{E}}_x(\boldsymbol{u}^0)$ and capillary pressure P_c^0/saturation S_w^0 is supplemented by the couple effective swelling stress $\boldsymbol{\Pi}_{eff}$/salinity C.

It should be noted that the triplet in the rhs of (79) constitutes our set of indpendent thermodynamic variables to describe isothermal chemo-mechanical coupled phenomena in unsaturated expansive media. The response constitutive functions (dependent variables) can be represented in terms of such set by the constitutive laws seated on the

micromechanical basis. Moreover, the essential features captured in the elastic case can be potentially extended to the elasto-plastic setting towards the representation of additional inelastic phenomena (e.g. chemical softening (Hueckel, 1992)).

4.8 Reduced cases

In what follows we examine the potential of the proposed approach in reproducing previous well-established models. To this end we begin by analyzing the two-scale model of a single microporous system. Denoting $k_s \to \infty$ the bulk modulus of the clay particles under the local incompressibility assumption, in the absence of distinction between nano- and micropores for a single porosity medium we have $\tilde{K}/K_s = \tilde{K}/k_s \approx 0$, which gives $\boldsymbol{\alpha} = \boldsymbol{I}$ and $\boldsymbol{\Pi}_{eff} = 0$ since the local characteristic length is much larger than the Debye's length of the EDL. Using these results in (64) we have $\boldsymbol{\chi}^{eff} = \chi^0 \boldsymbol{I}$ and the two-scale version of (65) reads as

$$\boldsymbol{\sigma}_T = \boldsymbol{\sigma}_E - P_a \boldsymbol{I} + \chi^0 P_c^0 \boldsymbol{I}\,, \tag{80}$$

which is nothing but the classical Bishop approach for a single-porosity unsaturated non-swelling medium (Coussy and Dangla, 2002; Pereira *et al.*, 2005; Nikooee *et al.*, 2013).

Finally, to reproduce the fully saturated case set $P_a = P_w^0$ and $P_c^0 = 0$ in (65) to obtain

$$\boldsymbol{\sigma}_T = \boldsymbol{\sigma}_E - P_w^0 \boldsymbol{I} - \boldsymbol{\Pi}_{eff}\,, \tag{81}$$

which recovers the result of Murad and Moyne (Murad and Moyne, 2008) under the absence of the air phase.

5 Self-consistent estimates

In order to validate the proposed approach computationally we shall henceforth combine the tools of periodic and self-consistent homogenization in order to construct straightforward simplified constitutive laws for the effective parameters for a particular spherical isotropic microstructure. According to the self-consistent approach of macroscopically isotropic media we consider a local arrangement of spherical clay clusters enclosing spherical micropores (Fig. 4). At the nanoscale, the clusters are composed of a radial arrangement of equally spaced parallel plane particles in order to ensure global isotropy which is in agreement with microstructures of face-to-face particles. Despite its simplifications, the physics underlying each parameter of the three-scale model is correctly captured and provides guidance for the development of more realistic models in random geometries. The procedure proposed herein allows to establish the relative roles of the electro-chemo-mechanical components at different length scales. In this arrangement, shear stresses vanish and the normal vectors exterior to the solid phase coincide with the radial unit vector $\boldsymbol{n} = \boldsymbol{N} = \mathbf{e}_r$.

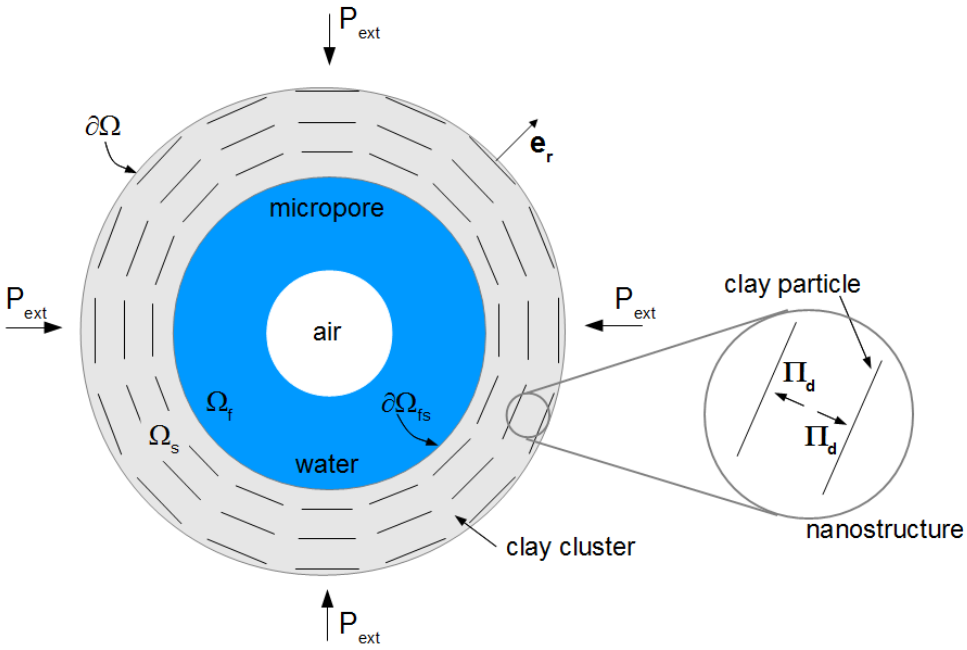

Figure 4: Isotropic microscopic cell structure.

Considering the macroscopic system subject to an external pressure $P_{ext} = -tr(\boldsymbol{\sigma}_T)/3$ our aim here is to provide constitutive response for some effective scalar coefficients, more precisely the bulk modulus of the solid matrix along with the volumetric parts of the swelling stress tensor (which we refer to as the swelling pressure), effective Bishop parameter and equivalent pore pressure.

5.1 Effective bulk modulus and Biot-Willis coefficient

For the isotropic geometry depicted in Fig. 4 the macroscopic Hooke's law reduces to $\boldsymbol{\sigma}_E = \lambda_s^T tr(\boldsymbol{\mathcal{E}}_x(\boldsymbol{u}^0))\boldsymbol{I} + 2\mu_s^T \boldsymbol{\mathcal{E}}_x(\boldsymbol{u}^0)$, with $\{\lambda_s^T, \mu_s^T\}$ the pair of macroscopic LamÃľ parameters. Hence, taking the trace and denoting $E = tr(\boldsymbol{\mathcal{E}}_x(\boldsymbol{u}^0))$, $\sigma_E = 1/3tr(\boldsymbol{\sigma}_E)$ and $\tilde{K} = \lambda_s^T + 2/3\mu_s^T$ the effective bulk modulus of the solid skeleton, we have

$$\sigma_E = \tilde{K} E \,. \tag{82}$$

The self-consistent homogenization method (Auriault *et al.*, 2009) aims at providing simplified analytical estimates for the effective coefficients based on Hill's Lemma, for instance the representation of the effective bulk modulus $\tilde{K}$ in terms of the porosity n_f and the bulk and shear modulus $\{K_s, \mu_s\}$ of the clay clusters (Hashin and Shtrikman, 1963; Hashin, 1983; Dormieux *et al.*, 2006). In the drained regime where the fluid phase has no impact on the elastic properties of the solid following the classical framework of

(Hashin and Shtrikman, 1963; Hashin, 1983), the self-consistent estimate of the effective bulk modulus can then be expressed as (Auriault *et al.*, 2009)

$$\frac{\tilde{K}}{K_s} = 1 - \frac{n_f}{1 - \dfrac{1-n_f}{1+\dfrac{4\mu_s}{3K_s}}} = 1 - \frac{n_f}{1 - \dfrac{1-n_f}{1+\dfrac{2(1-2\nu_s)}{1+\nu_s}}}\,, \tag{83}$$

where we assumed a constant Poisson coefficient ν_s of the clay clusters ($K_s/\mu_s = 2/3\,(1+\nu_s)/(1-2\nu_s)$). Using the above result in (66), the self-consistent estimate of the Biot-Willis coefficient is given by

$$\alpha = \frac{n_f}{1 - \dfrac{1-n_f}{1+\dfrac{4\mu_s}{3K_s}}} = \frac{n_f}{1 - \dfrac{1-n_f}{1+\dfrac{2(1-2\nu_s)}{1+\nu_s}}}\,. \tag{84}$$

5.2 Effective swelling pressure

In the sequel we exploit the same self-consistent approach to estimate the effective swelling pressure defined by the volumetric part of the swelling stress tensor $\Pi_{eff} = tr(\boldsymbol{\Pi}_{eff})/3$. Following the decomposition (63) for $\boldsymbol{\Pi}_{eff}$, the first term is the macroscopic average of the two-scale swelling stress tensor being identified with the disjoining pressure in a stratified nanostructure of equally spaced particles (10)

$$\left\langle \boldsymbol{\Pi}^0 \right\rangle = \langle \boldsymbol{\Pi}_d \rangle = \langle \Pi_d \rangle\, \boldsymbol{I} = (1-n_f)\Pi_d\, \boldsymbol{I}\,. \tag{85}$$

The second component is the average of the elastic stress $\boldsymbol{\Pi}_s = -\langle \boldsymbol{C}\boldsymbol{\mathcal{E}}_y(\boldsymbol{u}^1_\Pi)\rangle$ under the traction induced by $\boldsymbol{\Pi}^0$. For equally spaced particles within each cluster the term involving the dependence of $\boldsymbol{\Pi}_d$ with $\boldsymbol{y}$ in the closure problem for $\boldsymbol{u}^1_\Pi$ (53) vanishes and therefore exploring linearity with $\boldsymbol{\Pi}_d(\boldsymbol{x})$ we obtain in combination with (52) $\boldsymbol{u}^1_\Pi(\boldsymbol{x},\boldsymbol{y}) = -\boldsymbol{\xi}(\boldsymbol{y})\,\boldsymbol{C}^{-1}\,\boldsymbol{\Pi}_d(\boldsymbol{x})$. Hence, the electrochemical stress acting on the solid phase is written

$$\boldsymbol{\Pi}_s = \langle \boldsymbol{C}\,\boldsymbol{\mathcal{E}}_y(\boldsymbol{\xi})\rangle\, \boldsymbol{C}^{-1}\,\boldsymbol{\Pi}_d(\boldsymbol{x})\,. \tag{86}$$

Using (85) for $\left\langle \boldsymbol{\Pi}^0 \right\rangle$ along with the definition of the effective elasticity tensor $\boldsymbol{C}^{eff}$ (55) and assuming the independence of $\boldsymbol{C}$ on $\boldsymbol{y}$, we obtain the representation

$$\boldsymbol{\Pi}_{eff} := \left\langle \boldsymbol{\Pi}^0 + \boldsymbol{\Pi}_s \right\rangle = \langle \boldsymbol{C}\,(\boldsymbol{I}\boldsymbol{I} + \boldsymbol{\mathcal{E}}_y(\boldsymbol{\xi}))\rangle\, \boldsymbol{C}^{-1}\,\boldsymbol{\Pi}_d = \Pi_d\, \boldsymbol{C}^{eff}\boldsymbol{C}^{-1}\,\boldsymbol{I}\,. \tag{87}$$

For the isotropic microstructure of Fig. 4, we are mainly concerned by the volumetric part of the swelling stress $\Pi_{eff} = 1/3tr\,(\boldsymbol{\Pi}_{eff})$. Thus, in a similar fashion to the self-consistent estimate for linear-elasticity, using (84) we have

$$\Pi_{eff} := \frac{\tilde{K}}{K_s}\Pi_d = (1-\alpha)\Pi_d = \left[1 - \frac{n_f}{1 - \dfrac{1-n_f}{1+\dfrac{4\mu_s}{3K_s}}}\right]\Pi_d = \left[1 - \frac{n_f}{1 - \dfrac{1-n_f}{1+\dfrac{2(1-2\nu_s)}{1+\nu_s}}}\right]\Pi_d\,. \tag{88}$$

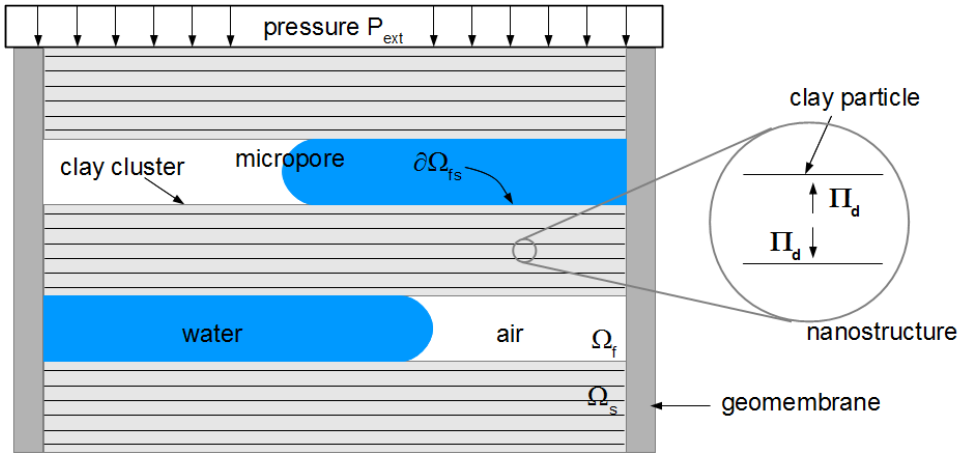

Figure 5: One-dimensional stratified cell structure.

The above result provides further insight in the three-scale swelling pressure Π_{eff}. The upper bound for the estimate (88) occurs in the stratified 1D arrangement of parallel clusters (Fig. 5) where $\Pi_{eff} = (1-n_f)\Pi_d$. The effects of the stress $\boldsymbol{\Pi}_s = -\langle \boldsymbol{C}\boldsymbol{\mathcal{E}}_y(\boldsymbol{u}^1_\Pi)\rangle$ are strongly tied-up to the cluster connectivity and tend to mitigate swelling compared to the stratified case. It should be noted that in the case of totally disconnected clusters $\boldsymbol{\Pi}_s = -\langle \boldsymbol{\Pi}^0 \rangle$ and from (63) $\boldsymbol{\Pi}_{eff} = 0$. Therefore the estimate provided by the self-consistent method satisfies $0 \leq \Pi_{eff}/\Pi_d \leq (1-n_f)$.

5.3 Effective Bishop parameter and equivalent pore pressure

Using the self-consistent estimates in (67) and (68), we obtain

$$\chi^{eff} = \frac{\tilde{K}}{K_s}(1-\chi^0) + \chi^0 = \left[1 - \frac{n_f}{1 - \dfrac{1-n_f}{1 + \dfrac{2(1-2\nu_s)}{1+\nu_s}}}\right](1-\chi^0) + \chi^0 \tag{89}$$

$$P_f^{eff} = \frac{tr(\boldsymbol{P}_f^{eff})}{3} = P_a - \chi^{eff} P_c \,. \tag{90}$$

The above result brings an extra constitutive dependence of χ^{eff} and P_f^{eff} on porosity n_f and the elastic property ν_s of the clusters. Note that $\chi^{eff} = \chi^0$ when $\nu_s = 1/2$ which corresponds to incompressible clusters.

5.4 Intra- and inter-cluster porosities

To complete the self-consistent estimates, for equally-spaced particles the intra-cluster $\phi = \langle \phi^0 \rangle^s = \phi(\boldsymbol{x})$ and inter-cluster $n_f = n_f(\boldsymbol{x})$ porosities are expressed in terms of the independent strain variables $\{E, S_w = S_w^0, C = C^0\}$. From (76), the mass balance of ϕ is given by

$$(1-n_f)(1-\phi) = (1-\bar{n}_f)(1-\overline{\phi})\exp(-E)\,. \tag{91}$$

To derive a self-consistent estimate for the inter-cluster porosity n_f, we begin by noting that for equally-spaced particles within each cluster swelling and disjoining stresses do not vary with the coordinate $\boldsymbol{y}$. Whence, by linearity we obtain the following reduced solution of (53)

$$\left\langle \boldsymbol{\nabla}_y \cdot \boldsymbol{u}_\Pi^1 \right\rangle = -\left\langle \boldsymbol{\nabla}_y \cdot \boldsymbol{\xi} \right\rangle \boldsymbol{C}^{-1}\boldsymbol{\Pi}_d \,, \tag{92}$$

Thus, from relation (72), using (60) to eliminate $\langle \boldsymbol{\nabla}_y \cdot \boldsymbol{\xi} \rangle$ along with micromechanical isotropic representation for the Biot-Willis parameter (Auriault and Sanchez-Palencia, 1977)

$$-\left\langle \boldsymbol{\nabla}_y \cdot \boldsymbol{\eta} \right\rangle = \frac{\alpha - n_f}{K_s}\,, \tag{93}$$

this yields

$$n_f = \bar{n}_f + (\boldsymbol{\alpha} - n_f \boldsymbol{I})\left[\boldsymbol{\mathcal{E}}_x(\boldsymbol{u}^0) - \boldsymbol{C}^{-1}\boldsymbol{\Pi}_d\right] + \frac{\alpha - n_f}{K_s}\left(1-\chi^0\right)P_c^0\,. \tag{94}$$

Moreover, using the classical relation $\alpha = 1 - \tilde{K}/K_s$ we obtain

$$n_f - \left(1 - \frac{\tilde{K}}{K_s}\right) = -\frac{n_f(1-n_f)}{\dfrac{2(1-2\nu_s)}{1+\nu_s} + n_f}\,, \tag{95}$$

so that combining the two above relations gives the constitutive laws for the inter-cluster porosity under uniform compression conditions

$$n_f = \bar{n}_f + \frac{n_f(1-n_f)}{\dfrac{2(1-2\nu_s)}{1+\nu_s} + n_f}\left(E + \frac{(1-\chi^0)P_c}{K_s} - \frac{\Pi_d}{K_s}\right) = \bar{n}_f + \frac{n_f(1-n_f)}{\dfrac{2(1-2\nu_s)}{1+\nu_s} + n_f} q\,, \tag{96}$$

with $q = q(E, S_w, C) := E + (1-\chi^0)P_c/K_s - \Pi_d/K_s$ a given function. The solution of (96) allows to build-up the constitutive response $n_f = n_f(E, S_w, C)$ parametrized by $\bar{n}_f$, K_s and ν_s.

5.5 Summary of the self-consistent results

Given $P_c = P_c(S_w)$, $\chi = \chi^0(S_w)$ and $\Pi_d = \Pi_d(C, \phi)$ for the isotropic microscopic cell geometry, in terms of the independent variables $\{E, S_w, C\}$ and parametrized by P_{ext}, $\bar{n}_f$, $\overline{\phi}$, K_s and ν_s the constitutive laws for the stress variables are given by

$$\begin{cases} -P_{ext} = \sigma_E - P_f^{eff} - \Pi_{eff} \\ \sigma_E = \tilde{K} E \\ P_f^{eff} = P_a - \chi^{eff} P_c \\ \chi^{eff} = (1-\alpha)(1-\chi) + \chi \\ \alpha = 1 - \dfrac{\tilde{K}}{K_s} \\ \Pi_{eff} = \dfrac{\tilde{K}}{K_s}\Pi_d = (1-\alpha)\Pi_d\,, \end{cases} \tag{97}$$

with

$$\frac{\tilde{K}}{K_s} = 1 - \frac{n_f}{1 - \dfrac{1-n_f}{1 + \dfrac{2(1-2\nu_s)}{1+\nu_s}}}\,, \tag{98}$$

and

$$\begin{cases} n_f = \bar{n}_f + \dfrac{n_f(1-n_f)}{\dfrac{2(1-2\nu_s)}{1+\nu_s} + n_f} q \\ (1-n_f)(1-\phi) = (1-\bar{n}_f)(1-\overline{\phi})\exp(-E)\,, \end{cases} \tag{99}$$

where $q = q(E, S_w, C) = E + (1-\chi)P_c/K_s - \Pi_d/K_s$.

6 Computational results

In what follows we illustrate numerically the multiscale approach by presenting simulations of the constitutive dependency of some effective parameters considering the isotropic microstructure of cluster arrangement with a stratified nanostructure of parallel particles within each cluster. The integral form of the local one-dimensional Poisson-Boltzmann problem is solved numerically adopting the discretization technique based on elliptic integrals (Moyne and Murad, 2006b). The input parameters of the simulations are: $\sigma = -0.2$ C.m^{-2}, $R = 8.314$ J.mol^{-1}.K^{-1}, $F = 96490$ C.mol^{-1}, $T = 293$ K, $\widetilde{\varepsilon}_0 = 8.854 \times 10^{-12}$ F.m^{-1}, $\widetilde{\varepsilon} = 80$, $\nu_s = 1/3$, and the capillary pressure is expressed as a function of the water saturation in the micropores S_w using a classical van Genuchten-type equation (Jacinto *et al.*, 2009)

$$P_c = P^* \left(S_w^{-1/\lambda} - 1\right)^{1-\lambda} , \tag{100}$$

with λ and P^* being empirical parameters. According to experimental studies performed by Jacinto et al. (Jacinto *et al.*, 2009) on MX80 bentonite samples choose $\lambda = 0.338$. To reduce the number of empirical parameters, pressures are displayed normalized with respect to the parameter P^*.

Figure 6(a) shows the effective Bishop parameter in (97) as a function of S_w for different values of α. From (67) as expected, for $\alpha = 1$ (corresponding to incompressible clusters) χ^{eff} is identical to its two-scale counterpart χ associated with a single-porosity medium. The gradual decrease in α leads to the appearance of the cluster compressibility and adsorbed water which tends to increase $\chi^{eff} \geq \chi$. It should be noted that unlike the transition to the fully-saturated regime where $\chi^{eff} = \chi = 1$, in contrast to χ, the effective parameter χ^{eff} does not vanish as $S_w \to 0$ but tends to the residual asymptotic value $1 - \alpha = \tilde{K}/K_s$ owing to the presence of the adsorbed water.

In Figure 6(b), we depict the effective equivalent pore pressure profiles $|P_f^{eff}/P^*|$ as a function of S_w for various values of α. For incompressible clay clusters $\alpha = 1$, the dual-porosity model tends to the single-porosity description with $P_f^{eff} \to P_f = P_a - \chi P_c$. In a similar fashion to χ^{eff} the decrease in α tends to increase the magnitude of P_f^{eff} compared to P_f with more pronounced disparity for low values of S_w.

Figure 7 depicts the effective swelling pressure as a function of salinity for different values of α. For incompressible clay clusters $\alpha = 1$, electrochemical effects arising from the nanopore level cannot be transmitted between adjacent clusters leading to $\Pi_{eff} = 0$. As the cluster compressibility increases ($\alpha \to 0$), electrochemical swelling becomes more pronounced, resulting in an increase of Π_{eff}. The fully-saturated case corresponding to the absence of micropores is parametrized by $\tilde{K} \to K_s$ and consequently $\alpha \to 0$. In this scenario the effective swelling pressure is maximum and identical to its microscopic

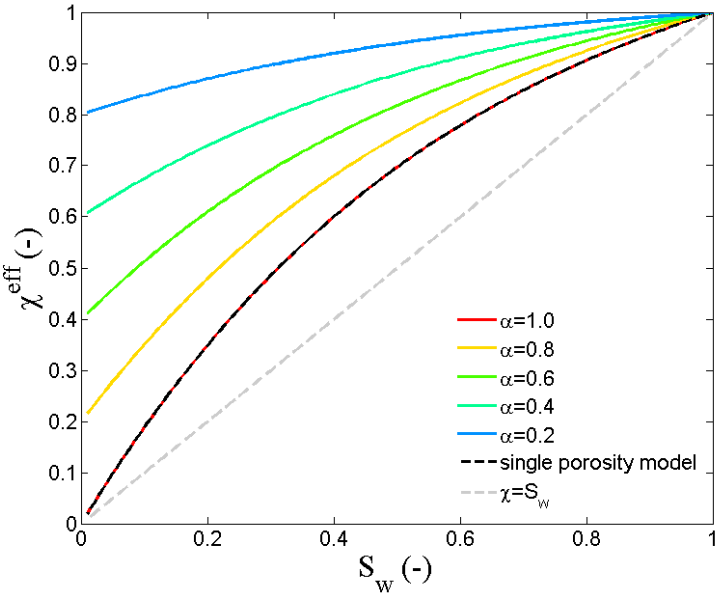

(a)

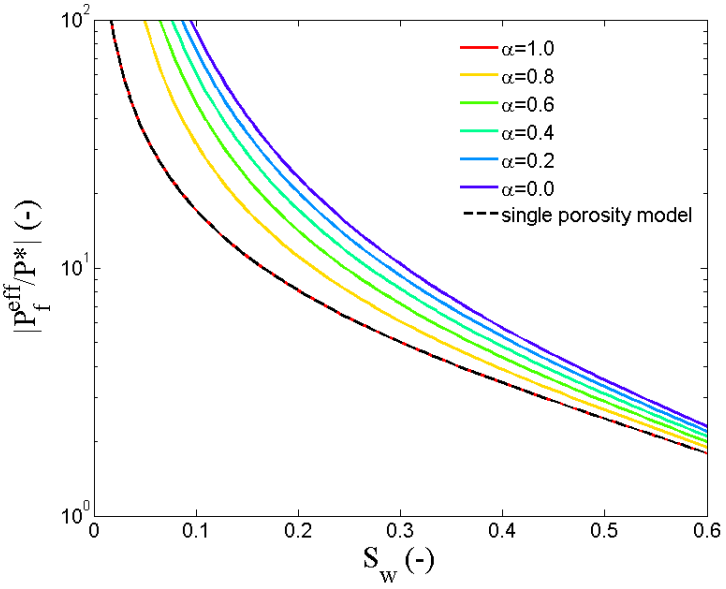

(b)

Figure 6: Effective Bishop parameter (a) and normalized effective equivalent pore pressure (b) as a function of S_w parameterized by α.

counterpart $\Pi_{eff} = \Pi = \Pi_d$ exhibiting a typical EDL profile (Murad and Moyne, 2002; Moyne and Murad, 2006b).

Using the self-consistent representation for α (84) along with the mass balance (91),

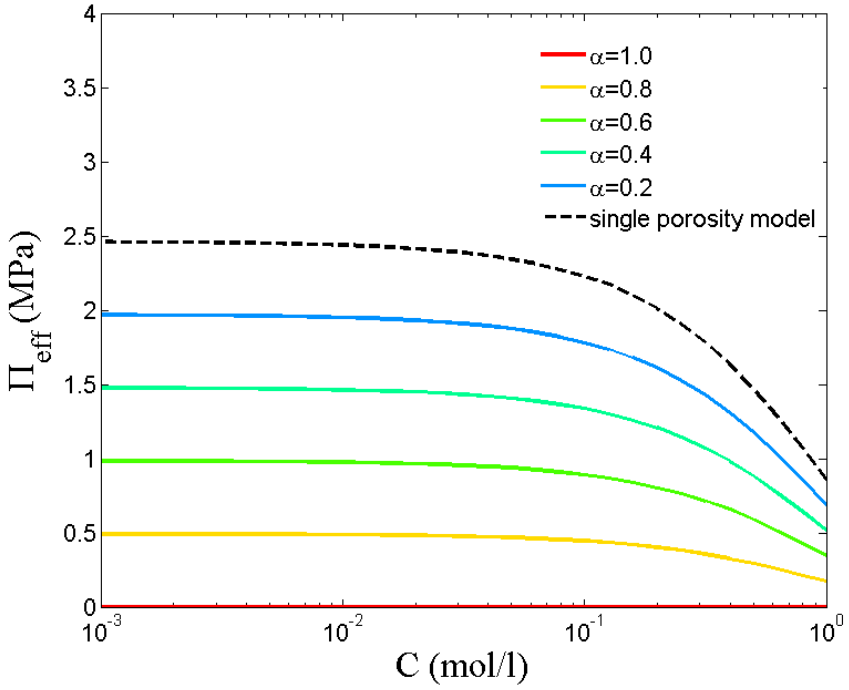

Figure 7: Effective swelling pressure as a function of salinity parameterized by α.

the effective parameters can also be represented as a function of the intra- and inter-cluster porosities. Fig. 8 depicts the effective Bishop parameter and equivalent pore pressure profiles χ^{eff} and $|P_f^{eff}/P^*|$ as a function of S_w for various values of ϕ at a fixed macroscopic strain with $E = 0$ for convenience, setting $\bar{n}_f = 0.7$ and $\overline{\phi} = 0.1$. As expected the additional amount of adsorbed water in the nanopores acts to decrease the Biot-Willis parameter α which from (97) also increases χ^{eff} and $|P_f^{eff}|$ tending to their classical two-scale profiles as $\phi \to 0$. Such illustration brings further insight in the characterization of the constitutive laws of $\{\chi^{eff}, P_f^{eff}\}$ in terms of the perturbations induced by the presence of the additional nanopore level.

Finally we analyze the impact of the perturbations induced by the micropore level on the swelling pressure computed from EDL theory under the presence of the nanopore system only. Fig. 9 depicts Π_{eff} as a function of C for various values of n_f. By invoking the mass balance (91) we impose $\phi = \overline{\phi} = 0.5$ and consider increase of n_f from $\bar{n}_f = 0.1$ induced by the volumetric strain E. As expected the increase of the micropore system dictated by high values of n_f tends to reduce the transmissibility of disjoining stresses between adjacent clusters, thus reducing the magnitude of Π_{eff} compared to Π_d.

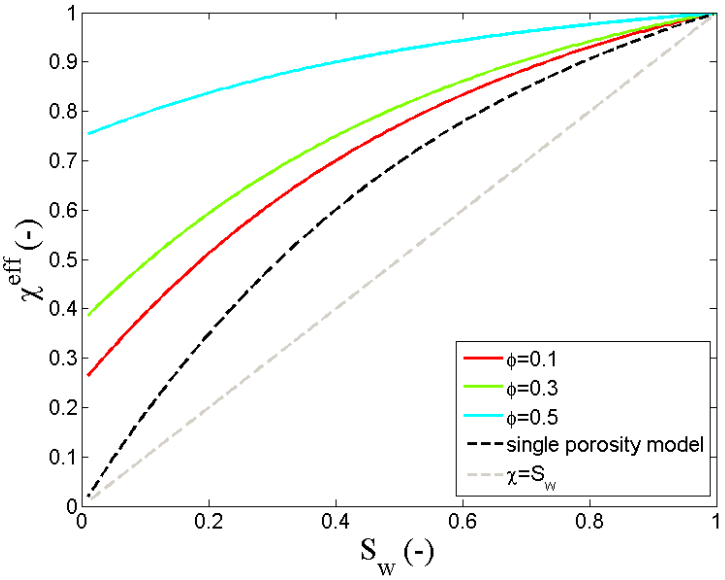

(a)

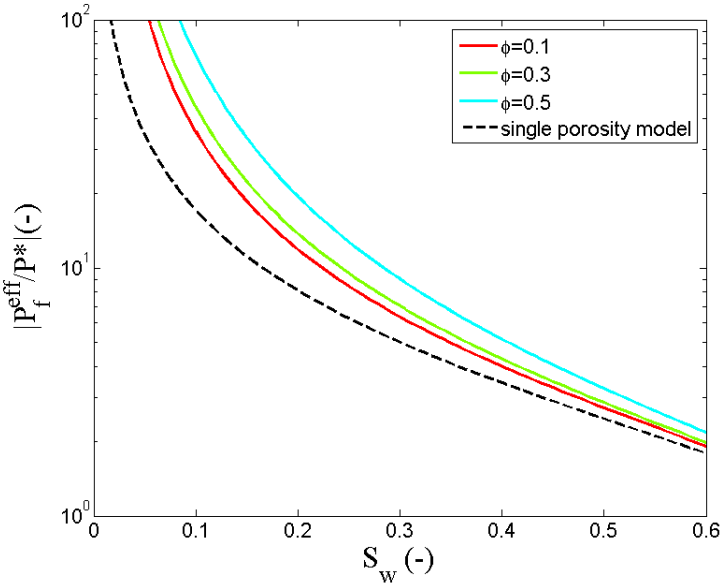

(b)

Figure 8: Effective Bishop parameter (a) and normalized effective equivalent pore pressure (b) as a function of S_w parameterized by ϕ; $E = 0$.

7 Conclusions

In this work we have successfully developed a three-scale model of unsaturated expansive clayey soils. The morphology of the swelling medium is characterized by two porous struc-

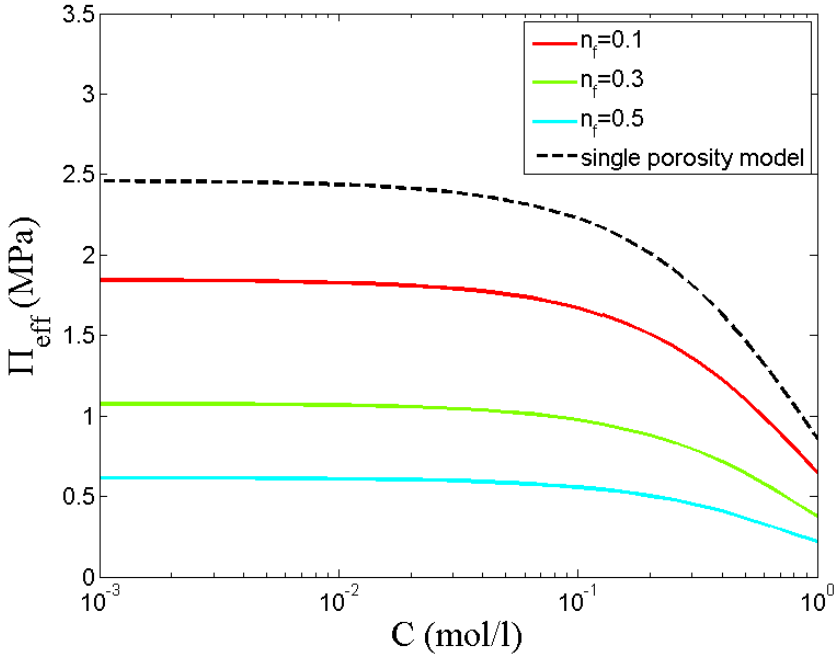

Figure 9: Effective swelling pressure as a function of salinity parameterized by n_f; $\phi = \overline{\phi} = 0.5$.

tures; the low permeable clay clusters with nanopores saturated by an electrolyte solution and the micropores filled by a mixture of bulk phase water and air. The clay cluster and the micropore systems are considered at mechanical and thermodynamic equilibrium characterized by the competition between disjoining forces of electrochemical nature and capillary attraction mechanisms.

By expressing the equilibrium of the bulk fluid in the micropores in terms of the equivalent pore pressure concept in the sense of Coussy and Dangla (Coussy and Dangla, 2002) the macroscopic model was rigorously derived within the asymptotic homogenization procedure applied to the microscale problem in conjunction with an electro-chemo-mechanical model for the clay aggregates based on Poisson-Boltzmann problem governing the electrochemistry of the electrolyte solution in the nanopores. The macroscopic governing equations incorporate a modified form of the effective stress principle accounting for a three-scale swelling stress tensor resulting from the EDL at the clay particle scale along with a modified three-scale Bishop parameter also accounting for the presence of adsorbed water. The modified effective stress principle can be rephrased in terms of the equivalent pore pressure which, likewise the Bishop parameter, differs from the two-scale version.

Exploring the tools of self-consistent homogenization the potential of the multiscale approach in capturing the coupled phenomena in the nano- and micropore levels was shown by numerical profiles of the effective parameters in the simplified geometry of an isotropic microstructure. Considering a particular form of nanostructure wherein each

spherical clay cluster is composed of parallel particles, the three-scale representations of the effective Bishop parameter and equivalent pore pressure reduce to their classical representation of single-porosity models in the case of incompressible clusters.

The proposed three-scale approach captures the correct physics underlying each electro-chemo-mechanical parameter and therefore provides new insight in the multiscale modeling of unsaturated swelling porous media. Although the computations were performed for a particular form of nano- and microstructure they provide guidance for further developments considering random geometries.

Acknowledgement: This work was supported by the funding provided by *Conselho Nacional de Desenvolvimento Científico e Tecnológico- CNPq* and by *Ministério da Ciência, Tecnologia e Inovação - MCTI* in the context of the Programa de Capitação Instutional – PCI/LNCC.

References

Achari G, Joshi RC, Bentley LR, Chatterji S (1999). "Prediction of the hydraulic conductivity of clays using the electric double layer theory." *Canadian Geotechnical Journal*, **36**(5), 783–792. doi:10.1139/cgj-36-5-783.

Alonso E, Gens A, Josa A (1990). "A constitutive model for partially saturated soils." *Géotechnique*, **40**(3), 405–430.

Alonso EE, Pereira JM, Vaunat J, Olivella S (2010). "A microstructurally based effective stress for unsaturated soils." *Géotechnique*, **60**(12), 913–925. doi:10.1680/geot.8.P.002.

Alonso EE, Vaunat J, Gens A (1999). "Modelling the mechanical behaviour of expansive clays." *Engineering Geology*, **54**(1-2), 173–183. doi:10.1016/S0013-7952(99)00079-4.

Auriault JL (1990). *Geomaterials: Constitutive Equations and Modelling*, chapter 14 Behaviour of porous saturated deformable media, pp. 311–328. Elsevier Science Publishers LTD.

Auriault JL, Boutin C, Geindreau C (2009). *Homogenization of Coupled Phenomena in Heterogeneous Media*. ISTE Ltd and John Wiley and Sons, Inc.

Auriault JL, Sanchez-Palencia E (1977). "Etude du comportement macroscopique d'un milieu poreux saturé déformable." *Journal de Mécanique*, **16**(4), 575–603.

Biot MA, Willis DG (1957). "The elastic coefficients of the theory of consolidation." *Journal of Applied Mechanics*, **24**, 594–601.

Bishop A (1959). "The principle of effective stress." *Lecture delivered in Oslo, Norway in 1955, published in Tecnisk Ukeblad*, **106**(39), 859–863.

Borja RI, Koliji A (2009). "On the effective stress in unsaturated porous continua with double porosity." *Journal of the Mechanics and Physics of Solids*, **57**(8), 1182–1193. doi:10.1016/j.jmps.2009.04.014.

Chateau X, Dormieux L (1995). "Homogenization of a nonsaturated porous-medium - Hills lemma and applications." *Comptes Rendus de l'Académie des Sciences Serie II Fascicule B – Mécanique Physique Chimie Astronomie*, **320**(12), 627–634.

Coussy O (2010). *Mechanics and Physics of Porous Solids*, chapter 6 - Surface energy and capillarity, pp. 107–146. John Wiley and Sons, Ltd.

Coussy O, Dangla P (2002). *Mécanique des Sols Non Saturés*, chapter 4 - Approche énergétique du comportement des sols non saturés, pp. 137–174. Lavoisier: Paris.

Coussy O, Pereira JM, Vaunat J (2010). "Revisiting the thermodynamics of hardening plasticity for unsaturated soils." *Computers and Geotechnics*, **37**(1-2), 207–215. doi: 10.1016/j.compgeo.2009.09.003.

Coussy OP, Brisard S (2009). "Prediction of drying shrinkage beyond the pore isodeformation assumption." *Journal of Mechanics of Materials and Structures*, **4**(2), 263–279. doi:10.2140/jomms.2009.4.263.

Derjaguin B, Churaev N, Muller V (1987). *Surface Forces*. Plenum Press, New York.

Dormieux L, Kondo D, Ulm FJ (2006). *Microporomechanics*. John Wiley and Sons, Ltd.

Fredlund D, Morgenstern N (1977). "Stress state variables for unsaturated soils." *Journal of the Geotechnical Engineering Division - ASCE*, **103**(GT5), 447–466.

Gallipoli D, Gens A, Sharma R, Vaunat J (2003). "An elasto-plastic model for unsaturated soil incorporating the effects of suction and degree of saturation on mechanical behaviour." *Géotechnique*, **53**(9), 844–844.

Gens A (1995). *Unsaturated Soils*, chapter Constitutive modelling: application to compacted soils, pp. 1179–1200. Balkema:Paris.

Gens A, Alonso EE (1992). "A framework for the behavior of unsaturated expansive clays." *Canadian Geotechnical Journal*, **29**(6), 1013–1032. doi:10.1139/t92-120.

Grant GP, Gerhard JI (2007). "Simulating the dissolution of a complex dense nonaqueous phase liquid source zone: 1. Model to predict interfacial area." *Water Resources Research*, **43**(12), W12410. doi:10.1029/2007WR006038.

Gray WG, Schrefler BA (2001). "Thermodynamic approach to effective stress in partially saturated porous media." *European Journal of Mechanics A-Solids*, **20**(4), 521–538. doi:10.1016/S0997-7538(01)01158-5.

Gray WG, Schrefler BA, Pesavento F (2009). "The solid phase stress tensor in porous media mechanics and the Hill-Mandel condition." *Journal of the Mechanics and Physics of Solids*, **57**(3), 539–554. doi:10.1016/j.jmps.2008.11.005.

Hashin Z (1983). "Analysis of composite-materials - A survey." *Journal of Applied Mechanics - Transactions of the ASME*, **50**(3), 481–505.

Hashin Z, Shtrikman S (1963). "A variational approach to the theory of the elastic behaviour of multiphase materials." *Journal of the Mechanics and Physics of Solids*, **11**(2), 127–140. doi:10.1016/0022-5096(63)90060-7.

Houlsby GT (1997). "The work input to an unsaturated granular material." *Géotechnique*, **47**(1), 193–196.

Hueckel T (1992). "On effective stress concepts and deformation in clays subjected to environmental loads - Discussion." *Canadian Geotechnical Journal*, **29**(6), 1120–1125. doi:10.1139/t92-130.

Hunter RJ (1981). *Zeta Potential in Colloid Science: Principles and Applications*. Academic Press, London; New York.

Huyghe JM, Janssen JD (1997). "Quadriphasic mechanics of swelling incompressible porous media." *International Journal of Engineering Science*, **35**(8), 793–802. doi:10.1016/S0020-7225(96)00119-X.

Huyghe JM, Janssen JD (1999). "Thermo-chemo-electro-mechanical formulation of saturated charged porous solids." *Transport In Porous Media*, **34**(1-3), 129–141. doi:10.1023/A:1006509424116.

Israelachvili JN (1991). *Intermolecular and Surface Forces*. Academic Press London.

Jacinto AC, Villar MV, Gomez-Espina R, Ledesma A (2009). "Adaptation of the van Genuchten expression to the effects of temperature and density for compacted bentonites." *Applied Clay Science*, **42**(3-4), 575–582. doi:10.1016/j.clay.2008.04.001.

Khalili N, Geiser F, Blight G (2004). "Effective stress in unsaturated soils: review with new evidence." *International Journal of Geomechanics*, **4**(2), 115–126. doi:10.1061/(ASCE)1532-3641(2004)4:2(115).

Laloui L, Nuth M (2009). "On the use of the generalised effective stress in the constitutive modelling of unsaturated soils." *Computers and Geotechnics*, **36**(1-2), 20–23. doi:10.1016/j.compgeo.2008.03.002.

Leverett MC (1941). "Capillary Behavior in Porous Solids." *Transactions of the AIME*, **142**(1), 152–169.

Loret B, Khalili N (2000). "A three-phase model for unsaturated soils." *International Journal For Numerical and Analytical Methods In Geomechanics*, **24**(11), 893–927. doi:10.1002/1096-9853(200009)24:11<893.

Loret B, Khalili N (2002). "An effective stress elastic-plastic model for unsaturated porous media." *Mechanics of Materials*, **34**(2), 97–116. doi:10.1016/S0167-6636(01)00092-8.

Moyne C, Murad M (2003). "Macroscopic Behavior of swelling porous media derived from micromechanical analysis." *Transport In Porous Media*, **50**(1-2), 127–151. doi:10.1023/A:1020665915480.

Moyne C, Murad MA (2002). "Electro-chemo-mechanical couplings in swelling clays derived from a micro/macro-homogenization procedure." *International Journal of Solids and Structures*, **39**(25), 6159–6190. doi:10.1016/S0020-7683(02)00461-4.

Moyne C, Murad MA (2006a). "A two-scale model for coupled electro-chemo-mechanical phenomena and Onsager's reciprocity relations in expansive clays: I Homogenization analysis." *Transport In Porous Media*, **62**(3), 333–380. doi:10.1007/s11242-005-1290-8.

Moyne C, Murad MA (2006b). "A two-scale model for coupled electro-chemo-mechanical phenomena and Onsager's reciprocity relations in expansive clays: II Computational validation." *Transport In Porous Media*, **63**(1), 13–56. doi:10.1007/s11242-005-1291-7.

Murad MA, Moyne C (2002). "Micromechanical computational modeling of expansive porous media." *Comptes Rendus Mecanique*, **330**(12), 865–870. doi:10.1016/S1631-0721(02)01543-7.

Murad MA, Moyne C (2008). "A dual-porosity model for ionic solute transport in expansive clays." *Computational Geosciences*, **12**(1), 47–82. doi:10.1007/s10596-007-9060-z.

Newman JS (1973). *Electrochemical Systems*. Prentice-Hall, Englewood Cliffs, N.J.

Nikooee E, Habibagahi G, Hassanizadeh SM, Ghahramani A (2013). "Effective stress in unsaturated soils: a thermodynamic approach based on the interfacial energy and hydromechanical coupling." *Transport In Porous Media*, **96**(2), 369–396. doi:10.1007/s11242-012-0093-y.

Nuth M, Laloui L (2008). "Effective stress concept in unsaturated soils: Clarification and validation of a unified framework." *International Journal For Numerical and Analytical Methods In Geomechanics*, **32**(7), 771–801. doi:10.1002/nag.645.

Pereira JM, Wong H, Dubujet P, Dangla P (2005). "Adaptation of existing behaviour models to unsaturated states: Application to CJS model." *International Journal For Numerical and Analytical Methods In Geomechanics*, **29**(11), 1127–1155. doi:10.1016/nag.453.

Sanchez-Palencia E (1980). *Non-Homogeneous Media and Vibration Theory*. Springer-Verlag, Berlin; New York.

Schreyer-Bennethum L (2007). "Theory of flow and deformation of swelling porous materials at the macroscale." *Computers and Geotechnics*, **34**(4), 267–278. doi: 10.1016/j.compgeo.2007.02-003.

Sheng D, Fredlund DG, Gens A (2008a). "A new modelling approach for unsaturated soils using independent stress variables." *Canadian Geotechnical Journal*, **45**(4), 511–534. doi:10.1139/T07-112.

Sheng D, Gens A, Fredlund DG, Sloan SW (2008b). "Unsaturated soils: from constitutive modelling to numerical algorithms." *Computers and Geotechnics*, **35**(6), 810–824. doi: 10.1016/j.compgeo.2008.08.011.

Sheng D, Sloan SW, Gens A (2004). "A constitutive model for unsaturated soils: thermomechanical and computational aspects." *Computational Mechanics*, **33**(6), 453–465. doi:10.1007/s00466-003-0545-x.

Vaunat J, Romero E, Jommi C (2000). "An elastoplastic hydro-mechanical model for unsaturated soils." In *Experimental Evidence and Theoretical Approaches in Unsaturated Soils, Proceedings of the International Workshop on Unsaturated Soils, Trento, Italy*, pp. 121–138. Balkema, Rotterdam.

Vlahinic I, Jennings HM, Andrade JE, Thomas JJ (2011). "A novel and general form of effective stress in a partially saturated porous material: The influence of microstructure." *Mechanics of Materials*, **43**(1), 25–35. doi:10.1016/j.mechmat.2010.09.007.

Wheeler SJ, Sharma RS, Buisson MSR (2003). "Coupling of hydraulic hysteresis and stress-strain behaviour in unsaturated soils." *Géotechnique*, **53**(1), 41–54. doi: 10.1680/geot.53.1.41.37252.